

Manuscript ID: tc-2017-54

Title: Implementing an empirical scalar tertiary anisotropy regime (ESTAR) flow relation into large-scale ice sheet models

Authors: Felicity Graham, Mathieu Morlighem, Roland Warner, and Adam Treverrow

Overall response to the reviewers

We thank the reviewers for their comments on our manuscript.

Both reviewers raise the important point of the need for further clarification in the manuscript on the definitions of anisotropy and tertiary creep. Specifically, reviewer 1 said:

The authors recall that the main aim of the paper is to present the implementation of ESTAR in an ice flow model and not to provide a comprehensive review of anisotropic flow models or a justification of ESTAR as it is presented in Budd et al. (2013). However as we may anticipate that this paper will mostly interest ice flow modellers that are not all specialist of ice rheology, I think that it is particularly important to correctly discuss the hypotheses of the flow law and what it can do or not.

And later on:

This do not prevent to implement ESTAR in a large-scale ice-sheet model and test its performances. But the different hypotheses and the character of the flow law must be described more carefully so ice flow modellers can discuss the choice of the flow law depending on the targeted applications. The authors should clarify and revise their use of both “anisotropy” and “tertiary creep” all along the manuscript.

We agree about the likely audience for this paper, and the importance of providing clear definitions about our use of the terms “anisotropy” and “tertiary creep”. Accordingly, we have rearranged and expanded the manuscript to clarify the discussion on these. We have introduced a new Sect. 2 that precisely defines anisotropy and the tertiary flow regime, and their relevance to polar ice sheets. We have introduced a new Sect. 3.4 that outlines those regions where our assumptions of anisotropy and tertiary creep, as they apply to the ESTAR flow relation, apply in polar ice sheets.

We have – as detailed in the specific responses to the reviewers below – changed our perspective on isotropy and anisotropy regarding flow relations. We have introduced a new Sect. 3.5 that differentiates between the anisotropic and isotropic flow relations that are used to describe the deformation of anisotropic ice. We acknowledge that the ESTAR flow relation is a mathematically isotropic flow relation that describes the flow of anisotropic ice. Accordingly, the acronym ESTAR now stands for Empirical Scalar Tertiary Anisotropy Regime (ESTAR).

We are glad that the reviewers agree that our work is of value. Indeed, we would be concerned if anyone regarded the use of the Glen flow relation as intrinsically superior to the ESTAR flow relation.

The modifications to address the reviewers’ concerns have been applied throughout the manuscript and we encourage the reviewers to consult the “diff” file we provide at the end of this response document.

We are confident that the substantial modifications we have made address the main concerns of the reviewers and provide sufficient background for readers.

Below, we have provided specific comments on the reviewer responses. In each, the reviewer comment is italicised, and our response is in normal font. We have provided direct quotations of the additions/modifications to the manuscript, where appropriate.

Kind regards,

Dr Graham and coauthors

REVIEWER 1

The primary concerns of reviewer 1 remain twofold. They are associated with:

1. the usage of the term anisotropy in connection with the ESTAR flow relation,
2. tertiary creep of ice in polar ice sheets, its connection with anisotropic crystal fabrics, and the validity of using observations from ice deformation experiments conducted in the laboratory to define a constitutive relation that is widely applicable to polar ice.

In the following we provide a response to the comments of reviewer 1, addressing specific points from the review where necessary.

Point 1: Anisotropic or not?

R1: ESTAR is then not an “anisotropic” flow relation, the fact that it predicts a different behaviour between compression and simple shear is not sufficient to comply with the definition of anisotropy.

We raised the question in our previous response as to whether there was more than a semantic difference between an anisotropic flow relation and a constitutive relation for ice with an induced anisotropy. After considering the reviewer’s latest comments we agree that the ESTAR flow relation is not an anisotropic flow relation, in the sense cited from various authorities, since it provides a constitutive relation that is unaffected by any hypothetical local rotation of the material.

We note that the new reviewer appears to consider this a suitable shift of perspective.

To avoid any confusion by readers we have modified the acronym, recasting it to describe the flow relation – Empirical Scalar Tertiary Anisotropy Regime (ESTAR) flow relation – to emphasise that this is a constitutive relation that describes the flow of anisotropic ice, not an anisotropic flow relation. We have also introduced a new Sect. 3.5 that discusses the differences between isotropic and anisotropic flow relations.

R1: Because ESTAR has no information about the material orientation, it does not enter this definition of anisotropy, as for a given solicitation (e.g. compression, simple shear) the material response will be invariant by any orthogonal transformation as, by definition, ESTAR does not include information about a material orientation. Contrary to what is claimed in response to reviewer 2, the scalar enhancement factor in ESTAR is an isotropic function of the deformability which itself is an isotropic function of the forcing represented by the deviatoric stress tensor and n (the normal to the non-rotating shear plane).

We agree with the reviewer’s terminology regarding absence of anisotropy in the constitutive relation, and in new Sect. 3.5 we have explained, for the benefit of “ice flow modellers that are not all specialists of ice rheology” that we are using an an isotropic constitutive relation to describe the deformation rates for ice with a deformation-induced anisotropic crystal fabric, as occurs during tertiary creep.

It is precisely to keep this restriction on the applicability of the ESTAR constitutive relation that we have carefully modified our acronym describing the constitutive relation to attach “anisotropy” to the ice in tertiary stage deformation rather than the flow relation (P2L34-P3L5):

“We refer to the generalised flow relation proposed by Budd et al. (2013) as ESTAR (Empirical Scalar Tertiary Anisotropy Regime), since it is based on steady-state (tertiary) creep rates describing the deformation of ice with a flow-compatible induced anisotropy and features a scalar (collinear) relationship between the strain rate and deviatoric stress tensor components.

As discussed below, the ESTAR relation is a mathematically isotropic flow relation for ice with a fully developed anisotropic fabric compatible with the deformation regime.”

As the new Sect. 3.5 makes clear, it is incorrect to assert that the ESTAR flow relation has no information about the material orientation. It is simply that we can only say (due to our foundations on actual experimental situations in tertiary flow) what the material properties are when the microstructure has evolved to be compatible with the stress configuration.

Our assumption that we are dealing with a fully developed deformation-induced anisotropy simply means that the material anisotropy has evolved to have a characteristic direction (\hat{n}) which can be predicted from the normal to the non-rotating shear plane. This is not conceptually different to measuring the axis of symmetry of a collection of crystal c -axes. The limitation is that unlike a microstructure based model, we cannot say what the deformations would be in response to an arbitrary applied stress – or equivalently an arbitrary rotation of the material.

In view of the public nature of The Cryosphere reviewing process we feel it worth making two further points here.

First, we suggest that if the flow relation had been presented with a unit vector \hat{n} simply declared as the axis of some material anisotropy, then the constitutive relation would be regarded as anisotropic. It is the immediate substitution into that flow relation of the normal to the non-rotating shear plane as the indicator of this axis of anisotropy (within the tertiary flow assumption) that collapses the anisotropic character of our constitutive relation.

Second, given the remark that “in general the anisotropic ice viscosity should be a rank-four tensor...” we feel it worth pointing out that if such a tensor description were developed as a similarly empirical constitutive relation for ice with a flow-induced anisotropy, that also would not constitute an anisotropic constitutive relation, since there would still be no sensitivity to material rotations. Note that such a tensor viscosity could have been constructed by more speculative extrapolations from the non-scalar analyses of the experiments on tertiary deformation rates under combined stresses presented by Budd et al (2013), or Warner et al (1999). Indeed, as we mention in the paper, the most general form of flow relation proposed by Glen (1958) on the basis of isotropy was not a scalar (collinear) flow relation.

R1: To summarise, I am not contesting that laboratory results shows that in tertiary creep the fabric depends only on the stress configuration and that the mechanical response depends on the fabric and thus on the stress configuration. ESTAR captures these properties and, integrated in an ice flow model, will give a spatially varying mechanical behaviour depending on the flow configuration. However, this is not the definition of anisotropy.

We have conceded that our usage of anisotropy with regard to the “rheology” or more specifically, the form of the ESTAR flow relation was potentially misleading, and we agree with the new reviewer that the usage of “rheology” should be restricted to the field of study and ought not be regarded as a synonym for a constitutive relation. However, we find it difficult to follow the reviewer’s logic that even though “... the mechanical response depends on the fabric ...” the reviewer does not regard this as having any connection with “anisotropy” of the deforming ice.

As the survey by the new reviewer shows, there are a variety of perspectives about the scope of the term “anisotropy”. We have included a new Sect. 2 in the updated manuscript that explicitly defines what we mean by anisotropy and polar ice sheets, and a new Sect. 3.5 that discusses the distinction between anisotropic flow relations and the flow of anisotropic ice in the context of tertiary flow.

R1: In consequence the manuscript must be revised to use the term “anisotropy” where appropriate, especially it can not be included in the acronym to describe the flow law.

Precisely because “this paper will mostly interest ice flow modellers that are not all specialist of ice rheology”, we consider it is important to keep the fact of the deformation-induced anisotropic fabric of the polycrystalline ice in our revised acronym to emphasise that the effects we are treating and the domain of applicability of our constitutive relation only concerns the tertiary flow of ice with a flow-induced anisotropy (new Sects. 2 and 3.5). In relation to the ESTAR flow relation – our descriptive characterisation of the flow relation from Budd et al. (2013) – we emphasise that this is an empirical scalar flow relation, describing the deformation of ice in the state of tertiary anisotropy. Hence the ESTAR flow relation – Empirical Scalar Tertiary Anisotropy Regime.

Point 2: Tertiary creep and anisotropy

Main points:

- To improve clarity, a new Sect. 2 has been added in which we articulate our usage of anisotropy and describe tertiary flow.
- We have clarified our remarks about tertiary creep being commonly encountered in polar ice sheets, particularly in regions that strongly control the large-scale dynamics, and we have also expanded our remarks about regions where our model assumptions would not apply (Sect. 3.4). Indeed, in the previous revision we already addressed this – highlighting problematic regions arising in the simulations (e.g., throughout the Discussion).

Comments on the activity of migration recrystallisation

It is worth noting that, like the reviewer, we consider that multiple microdeformation and recovery mechanisms contribute to the creep deformation of polar ice, and that the relative contribution of individual processes may be expected to vary spatially throughout an ice sheet due to the influence of temperature and/or stress on their activity.

Differences of opinion emerge when it comes to the activity of migration recrystallisation. The reviewer suggests that tertiary creep rates from laboratory experiments have only limited relevance to in-situ conditions because migration recrystallisation is active under laboratory conditions, but not under in-situ conditions. In contrast to this, our view is that recovery processes enabling grain boundary migration do make a contribution to microstructural development within ice sheets.

Reviewer 1 states:

For the applicability of ESTAR, the question is then not too much ‘is tertiary creep occurring?’ but ‘is tertiary creep as seen in laboratory experiments where migration recrystallisation is important occurring?’. The answer is clearly related to the activity of migration recrystallisation in-situ.

And later on:

I then maintain that the occurrence of migration recrystallisation and its importance in controlling the microstructure evolution, is an important observation to assess areas where in-situ conditions could be compared to the laboratory tests that have been used to calibrate ESTAR.

If, as suggested, the activity of migration recrystallisation is key to determining the validity of using laboratory observations to specify a constitutive relation for polar ice sheets, then it is necessary to assess where any such threshold lies. If all microdeformation and recovery processes in polycrystalline

ice were adequately understood it would be possible to describe any variability or thresholds in their activity. In general this is not the case, and in the absence of a generally agreed threshold for the activity of migration recrystallisation, we return to the example from Law Dome, described in our initial response to the reviews as a guide (also discussed in Sect. 2 of the updated manuscript). We reiterate that for the A001 core drilled at the dome summit, a distinct small circle girdle (cone-type) fabric is observed at a depth of 318 m, where the total accumulated strain is $\sim 30\%$ and the in-situ flow regime is compression dominated, with approximately radial symmetry in the transverse rates (Fig. 3a, Budd and Jacka, 1989). The latter is supported by observations from the Dome Summit South drill site and borehole, ~ 4 ice thicknesses downstream of A001. The in-situ temperature within this zone is $\sim -22^\circ\text{C}$. The important points from this are that:

- a cone-type fabric such as this cannot form by lattice rotation alone in a compression dominated setting, therefore boundary migration processes must be contributing to microstructural development in a relatively low temperature setting
- similar fabrics cone-type fabrics are also observed in uniaxial compression laboratory experiments that are conducted at higher temperatures and stresses than those encountered in-situ.

From these observations we can infer that migration recrystallisation is both active and influential under in-situ conditions – at least for temperatures as low as $\sim -22^\circ\text{C}$. As such, a crude approximation for the activity of migration recrystallisation and a limit for extrapolating laboratory observations down to in-situ conditions might be $\sim -22^\circ\text{C}$. This temperature is almost certainly an upper limit. Cone-type fabrics have been observed in what are expected to be compression dominated settings at other locations, e.g. cores drilled at Siple Dome (DiPrinzio et al., 2005), Byrd (Gow and Williamson, 1976), Dye 3, Greenland (Herron et al., 1985) and the Amery (Budd, 1972) and Ross ice shelves (Gow, 1963). The corresponding in-situ temperatures are even lower for some of these sites, suggesting that migration recrystallisation remains sufficiently active to influence microstructure at temperatures below $\sim -22^\circ\text{C}$.

From the examples given above and those presented within Sects. 2 and 3.4 of the manuscript, there is sufficient evidence to support our view that the ESTAR flow relation is likely to be applicable in the dynamically active regions of the ice sheet where creep deformation makes a significant contribution to overall flow. The task of identifying the cutoffs where the ESTAR flow relation may cease to be applicable e.g., in less dynamically active zones of the ice sheet, remains an active area of research.

Further comments on using laboratory data in the development of constitutive relations

When it comes to the implementation of the ESTAR flow relation, a detailed discussion in response to the reviewers question ‘is tertiary creep as seen in laboratory experiments where migration recrystallisation is important occurring?’ while relevant, is of secondary importance. Of greater relevance is whether or not the values of enhancement prescribed by the ESTAR flow relation – which are derived from experiments – are applicable to in-situ conditions.

The reviewer states:

In their reply, the authors seem to suggest that the development of fabrics is a proof of the existence of tertiary flow. I don't see the causality, as the plastic deformation by slip induce an evolution of the fabric, so there is no requirement to reach the tertiary creep to have a fabric.

Some clarifying remarks on anisotropy and tertiary creep are required here. We did not intend to suggest that one had to reach tertiary creep to have anisotropic fabric. It is true, we do not have

to reach tertiary creep to have an anisotropic fabric. However, the strain induced development of an anisotropic fabric is an integral part of reaching tertiary creep (where tertiary creep corresponds to the point where the microstructure (and strain rate) have evolved to be compatible with the imposed stresses). We assume that microstructural anisotropy is the cause of the different deformation responses observed for different stress regimes. If and when the stress configuration changes the microstructure will evolve in order to establish a new tertiary creep state.

Since the ESTAR flow relation is an empirical relationship used to define an enhancement factor dependent on the stress configuration, it will work provided the nature of mechanical anisotropy identified in experiments is consistent with in-situ conditions. It would not be possible to sensibly apply the ESTAR flow relation to simulating ice sheet dynamics if it was possible to point to widespread regions in an ice sheet where the fabric has evolved in such a way as to reduce the bulk deformation rate below that which would be expected from ice with an isotropic fabric. To our knowledge there are no ice core (fabric) and corresponding borehole deformation (other in situ measurements) that support the concept of widespread hardening in response to fabric evolution.

We do not suggest that the ESTAR flow relation is the final word on simulating anisotropic polar ice (Introduction, P3L5-7). We use the ESTAR flow relation on the basis that it provides better overall performance in simulating ice sheet dynamics than the Glen flow relation. There will be regions where the ESTAR flow relation is not applicable; however, we make it clear in the manuscript where we think it will and will not work, and comment on the relative importance of these zones to the overall dynamics of an ice sheet (Sect. 3.4). For example, the ESTAR flow relation may overestimate strain rates in the coldest, near surface layers of the deep interior of a polar ice sheet where accumulated strains are low (P10L19-26). Since strain rates are correspondingly low in such regions the overall impact of ‘getting it wrong’ here will be minimal. We discuss the significance of ‘getting it wrong’ in the new Sect. 3.4.

Lastly, the use of laboratory data to constrain constitutive relations is not unique to the ESTAR flow relation. At some level, most if not all flow relations are based on, calibrated by, or validated using experimental results. In many cases (including the ESTAR flow relation) specification of the limiting values of strain rate enhancement associated with the development of fabrics are obtained from laboratory results, so the ESTAR flow relation sets no new precedent here. Furthermore, the prescription of the temperature dependence of ice flow rates that is commonly used in many models is based on experimental secondary creep rates.

The strain required for the development of tertiary creep

It is clear from many laboratory studies that tertiary creep occurs at strains of $\sim 10\%$ – we regard this as a lower limit. Since this was not already clear in the manuscript we now indicate that tertiary creep occurs at $\geq 10\%$ strain (Sect. 2, e.g., P4L18-32).

There are suggestions that the strain required to develop steady-state strain rates and compatible fabrics at lower temperatures and stresses may be higher than values obtained from laboratory experiments. In the example from the Law Dome A001 ice core described above, a distinct cone-type fabric is observed for a strain of $\sim 30\%$, providing an upper limit for the strain required to develop a compatible fabric under in-situ conditions. Since the fabric is already well developed at this point, the actual strain required to achieve tertiary creep was probably less. This idea is further supported by experimental observations (Jacka and Maccagnan, 1984) that show how a steady-state (tertiary) creep rate is achieved prior to corresponding anisotropic fabric reaching a steady-state. The suggestion here is that the strain rate does not continue to evolve so much once the most obstructive grains have been

removed by fabric development, i.e. the continued strengthening of an already anisotropic fabric has a minor influence on the strain rates. We discuss this result in new Sect. 2.

While the experiments of Jacka and Li (2000) cited by the reviewer provide some support for the requirement of higher accumulated strains to develop tertiary creep at low temperatures and stresses, the results of these experiments are somewhat inconclusive and should be interpreted with care. These experiments were conducted at constant applied loads, not constant applied stresses. Due to an increase in the cross sectional area of the sample with increasing strain the stress effectively decreases throughout the experiments. This effect can be observed by the decrease in creep rates at strains $\geq 10\%$ for the higher temperature and/or stress experiments (see their Figures 7 & 8). At a strain of 10% the corresponding decrease in stress will lead to strain rates $\sim 30\%$ lower than the value expected for the stress that was applied at the start of the experiment. From this perspective the nearly constant strain rates referred to by the reviewer actually indicate a modest (30%) enhancement in the flow relation by 10%. Accordingly, we suggest that the cone-type fabric from A001 at $\sim 30\%$ and $\sim -22^\circ\text{C}$ provides a more robust indication of the levels of strain required for fabric development (Sect. 2, P4L33-P5L8).

Throughout much of an ice sheet the evolution in the stress configuration and corresponding compatible microstructure along ice streamlines is gradual, hence the strain required for the microstructure to adapt to changes is substantially less than observed in laboratory experiments that commence on samples with an initially isotropic fabric.

REVIEWER 2

From Section 2.1: Scientific points (July 2017):

R2: I think it might be helpful to include a short section in the Introduction to address [the semantics of anisotropy] head-on, as outlined in the following item. This could come at the expense of removing some to the other introductory material about anisotropy, which I felt didn't always make the point that is needed here.

Perhaps if the authors can clarify exactly what they mean by an anisotropic flow relation in this paper with a few sentences or paragraphs, it will convince readers to focus on their results, and their paper will be more widely cited. I expect that glaciologists agree that ice develops a non-uniform preferred crystal orientation fabric as a result of deformation, and that because an ice crystal has essentially just one slip system, this preferred crystal orientation fabric affects the deformation rate.

We greatly appreciate the considerable effort expended by the reviewer in detailing each of the different concepts of what might be meant by an “anisotropic flow relation”. In the revised manuscript we have adopted this reviewer’s original perspective that (Introduction, P3L4-5):

“...the ESTAR relation is a mathematically isotropic flow relation for ice with a fully developed anisotropic fabric compatible with the deformation regime.”

Accordingly, we have amended the acronym to now stand for: Empirical Scalar Tertiary Anisotropy Regime, intending the usage “ESTAR flow relation” to correspond to “Glen flow relation”. We have added a new Sect. 2 to discuss anisotropy and polar ice sheets, both the experimental and observational evidence, and the importance of its consideration in constitutive relations for use in numerical ice sheet models. For completeness, and in line with the reviewer’s recommendation from both reviews, we have also added a new Section 3.5 to discuss the seeming paradox of using an isotropic constitutive relation to describe the flow of ice with a deformation-compatible tertiary anisotropic crystal fabric. We have added this at the end of the section on constitutive relations, rather than in the introduction. Given that we have adopted the reviewer’s suggested perspective of presenting the ESTAR flow relation as a mathematically isotropic flow relation for anisotropic ice, we consider that this was the appropriate place to put this discussion.

R2: I am puzzled by Equation (21), which represents the incoming boundary condition for flow. Equation (21) does not go to zero at the lateral boundaries ($x = 0$ and $x = L$), yet the boundary condition along the lateral margins is zero flow, i.e., $v_y(0, y) = v_y(L, y) = 0$. Since $x_{mid} = L/2$, these two conditions are incompatible in the corners where they meet. Admittedly, $\exp(-5.96) = 0.003$ is small, but it is not zero. Does this create some of the fine structure there, for example in Figure 4a?

In the original set of experiments, we subtracted the small value of v_y at $x = 0$ and $x = L$ to ensure that v_y satisfies the no-slip boundary condition at the margin. We have revised the manuscript to be clear on this, as follows (P15L9-13):

“At the inflow boundary, the y -component of velocity is set by

$$V(x) = V_0 e^{-\left[\frac{5(x-x_{mid})}{2L}\right]^8}, \quad (1)$$

$$v_y(x, 0) = V(x) - V(0), \quad (2)$$

where $V_0 = 100 \text{ m yr}^{-1}$ and $x_{mid} = L/2$. This ensures that $v_y(x, 0)$ satisfies the no-slip boundary condition on the margins.”

R2: It is a pity that the ISMIP experiments used only sinusoidal bed variations, because, as the authors point out, they are unable to examine the ESTAR response in what we might call the far field,

away from the influence of an isolated bump. Perhaps in future work, experiments with isolated bumps in a longer model domain would shed more light on the effectiveness of the ESTAR formulation?

We agree with the reviewer and are planning further tests of the ESTAR flow relation over synthetic and realistic domains. It would certainly be desirable to decouple the spatial scale of a bump from any effects of periodic boundary conditions.

From Section 2.2: Editorial points and clarity (July 2017):

R2: Page 9, line 10: binormal to a flow line

A binormal to a flow line has been defined (P12L17) as “the unit vector orthogonal to both the tangent vector and the normal vector”. Throughout the manuscript, we have amended flow-line/flowline to flow line, unless where the word streamline is more appropriate.

R2: Page 11, line 11: Consistent with what theory?

Our results are consistent with those predicted from Ern and Guermond (2004), as discussed also on P12L22-26. This reference has been added on P14L18.

R2: Page 21, line 25: Should be Fig. 3f.

Amended (P15L28).

R2: Can times be slow?

Amended (P16L23).

R2: Misplaced only

Amended.

R2: Extensive/extensile/tensile

We have removed all occurrences of *extensive*, instead adopting *tensile* or *extensional*, where appropriate. E.g., see P15L23-24 and P16L4-5.

R2: Flow line/streamline/particle path

We have replaced flow line with streamline throughout the manuscript.

R2: Hyphens

We have removed hyphens on computationally efficient, and added a hyphen to near-surface (P10L21).

R2: Figure 1 axes

We have amended Fig. 1 axes labels as suggested. The x-axis is strain, but plotted on a log scale. The y-axis (strain rate) is also plotted on a log scale and the units have been removed from the label. We have specified that this figure is intended to be a cartoon to illustrate the relationships between strain and strain rates for different stress regimes and at different stages of deformation.

R2: Use of e notation on graphs

We have removed all occurrences of the e notation on graph axes.

From Section 3.1: Scientific points (March 2017):

R2: It would be fair to say that ESTAR offers an improved flow law for ice that is anisotropic, but it is incorrect to say that ESTAR is an anisotropic flow law

We agree with the reviewer. As mentioned above in response to the scientific points from the reviewer’s section 2.1, we have removed all reference to the ESTAR flow relation as an anisotropic flow

relation. Rather, we clarify that the ESTAR flow relation is a mathematically isotropic flow relation for describing the influence of induced anisotropy (P3L4-5).

R2: “Data from laboratory ice deformation experiments can be used to define flow relations suitable for implementation in numerical ice sheet models.” This may be correct, but at such dramatically different rates of strain, isn’t there a strong possibility that the dominant micro-scale processes are different, and if that’s the case, why should the lab experiments offer very much insight? Some more discussion might be in order.

We have made detailed comments related to this same issue in our response to reviewer 1 above: “Further comments on using laboratory data in the development of constitutive relations”. To briefly summarise: laboratory results are broadly transferable to polar ice sheets, particularly the dynamically active zones, but identifying thresholds in the activity of specific microdeformation and recovery processes (in order to determine when laboratory observations are no longer representative of in-situ conditions) remains an area of active research. In the updated manuscript we have added discussion about the rates of strain observed in laboratory experiments of tertiary creep and how they compare with observations from the field (e.g., from the A001 core drilled at the Law Dome summit; Budd and Jacka, 1989; Sect. 2 of the updated manuscript), as well as the applicability of laboratory experiments in constraining and validating constitutive relations (Sects. 3.2 and 3.4).

R2: Both previous reviewers expressed concern that ESTAR is based on the assumption that tertiary creep has been reached everywhere. This is equivalent to the expectation that there is “an anisotropic flow relation for polycrystalline ice in which the nature of the crystal fabric and the magnitude of strain rate enhancement, E , are both determined by the stress regime.” I think we all understand that fabric actually evolves in response to strain, so in order for these two different views to be compatible, the time required for ice to undergo $\approx 10\%$ strain must be significantly less than the time required for it to move into a regime with a significantly different stress. Perhaps the paper by Thorsteinsson et al. (2003) would offer some ideas and discussion points about where this might be justified and where not.

We thank the reviewer for the insightful reference (Thorsteinsson et al., 2003) that highlights situations where the ESTAR flow relation might not apply. We have incorporated this reference in new Sect. 3.4, which outlines the domain of applicability of the ESTAR flow relation, and where the assumptions underlying the ESTAR flow relation are not expected to hold.

In the first revision of the paper we had already made efforts to indicate the type of region where this compatibility of anisotropy and stress regime was unlikely to be justified, and to address the connection between the time required to develop a compatible fabric (in terms of accumulating strain), the distance travelled in that time and the spatial scales over which the stress regime might change significantly. In the Discussion section we explicitly introduced the concept of a transition scale – the distance travelled in accumulating $\sim 10\%$ strain and used this to draw attention to regions in the simulations where the assumption of tertiary flow with a compatible fabric was expected to fail.

In the current version we have further expanded on this matter in the Sects. 2 and 3.4, as well as retaining the remarks in the Discussion section – e.g., P22-23.

R2: Figure 1 caption. “Note that the ratio...is approximately 8/3...” How is a reader suppose to note this when there are no numbers on the vertical axis? The figure is just a cartoon.

We have amended the caption on Fig. 1 and made the intent of the figure more explicit.

From Section 3.2: Editorial points (March 2017):

R2: Some purists would say that rheology denotes a field of study, like geology, and a better term in

the title would be constitutive relation.

We agree with the reviewer and have replaced “rheology” with “constitutive relation” or “flow relation” throughout the manuscript.

R2: Cuffey and Paterson (2010) and Paterson (1994) references need page numbers

We have added a page number to both the Cuffey and Paterson (2010) and Paterson (1994) references.

R2: Section 4 not mentioned in outline, although all other sections are mentioned.

Amended (P3L13-20).

R2: Avoid long strings of adjectives

Amended as suggested.

R2: Misplaced “only”s

Amended.

R2: Definition of NRSP moved before idea of simple shear

We have reordered the material in section 3.3 so that the discussion of the non-rotating shear plane and the shear acting on that plane is introduced before the shear fraction is formally defined (P8-9).

R2: Taylor Hood and $P1 \times P1$ elements

We have specified the type of finite elements used in the verification process as it is a relevant detail for replicability, especially for modellers hoping to implement the ESTAR flow relation into their own models. Should readers require more information, details on the finite element method are provided in the reference (Ern and Guermond, 2004), and the ISSM code is available online.

R2: ...In this case, eliminating the acronyms HO (higher order) and FS (full Stokes) and just writing those terms out in full for the perhaps 2 dozen times they are used would make the paper more readable...

We agree with the reviewer and have removed the acronyms HO and FS.

References

- Budd, W. and Jacka, T.: A review of ice rheology for ice sheet modelling, *Cold Reg. Sci. Technol.*, 16, 107–144, 1989.
- Budd, W. F.: The development of crystal orientation fabrics in moving ice, *Z. Gletscherkd. Glazialgeol.*, 8, 65–105, 1972.
- Budd, W. F., Warner, R. C., Jacka, T. H., Li, J., and Treverrow, A.: Ice flow relations for stress and strain-rate components from combined shear and compression laboratory experiments, *J. Glaciol.*, 59, 374–392, doi:10.3189/2013JoG12J106, 2013.
- DiPrinzio, C., Wilen, L., Alley, R., Fitzpatrick, J., Spencer, M., and Gow, A.: Fabric and texture at Siple Dome, Antarctica, *J. Glaciol.*, 51, 281–290, 2005.
- Glen, J.: The flow law of ice: A discussion of the assumptions made in glacier theory, their experimental foundations and consequences, *IASH Publ.*, 47, 171–183, 1958.
- Gow, A.: The inner structure of the Ross Ice Shelf at Little America, Antarctica, as revealed by deep core drilling, in: *IUGG General Assembly of Berkeley*, pp. 272–284, IASH Publ. No. 61, 1963.
- Gow, A. and Williamson, T.: Rheological Implications Of Internal Structure And Crystal Fabrics Of West Antarctic Ice Sheet As Revealed By Deep Core Drilling At Byrd-station, *Geol. Soc. Am. Bull.*, 87, 1665–1677, 1976.
- Herron, S., Langway, Jr, C., and Brugger, K.: Ultrasonic velocities and crystalline anisotropy in the ice core from Dye 3, Greenland, in: *Greenland ice core : geophysics, geochemistry, and the environment*, edited by Langway, Jr, C., Oeschger, H., and Dansgaard, W., no. 33 in *Geophysical monograph*, pp. 23–31, American Geophysical Union, 1985.
- Jacka, T. and Li, J.: Flow rate and crystal orientation fabrics in compression of polycrystalline ice at low temperatures and stresses, in: *Physics of Ice Core Records*, edited by Hondoh, T., pp. 83–101, The Institute of Low Temperature Science, Hokkaido University, Sapporo, Hokkaido University Press, Sapporo, 2000.
- Jacka, T. and Maccagnan, M.: Ice crystallographic and strain rate changes with strain in compression and extension, *Cold Reg. Sci. Technol.*, 8, 269–286, 1984.
- Thorsteinsson, T., Waddington, E. D., and Fletcher, R. C.: Spatial and temporal scales of anisotropic effects in ice-sheet flow, *Ann. Glaciol.*, 37, 40–48, 2003.

Implementing an empirical scalar ~~tertiary anisotropic rheology (ESTAR)~~ constitutive relation for ice with flow-induced polycrystalline anisotropy into large-scale ice sheet models

Felicity S. Graham¹, Mathieu Morlighem², Roland C. Warner³, and Adam Treverrow³

¹Institute for Marine and Antarctic Studies, University of Tasmania, Private Bag 129, Hobart, Tasmania 7001, Australia

²Department of Earth System Science, University of California, Irvine, California, USA

³Antarctic Climate and Ecosystems Cooperative Research Centre, Private Bag 80, Hobart, Tasmania 7001, Australia

Correspondence to: Felicity S. Graham (felicity.graham@utas.edu.au)

Abstract. ~~The microstructural evolution that occurs in polycrystalline ice during deformation leads to the development of anisotropic rheological properties that are~~ microstructure of polycrystalline ice evolves under prolonged deformation, leading to anisotropic patterns of crystal orientations. The response of this material to applied stresses is not adequately described by the ~~most common, isotropic,~~ ice flow relation ~~most commonly~~ used in large-scale ice sheet models – the Glen flow relation. We present a preliminary assessment of the implementation in the Ice Sheet System Model (ISSM) of a ~~computationally efficient~~ computationally efficient, empirical, scalar, ~~tertiary, anisotropic rheology (ESTAR)~~ constitutive or flow relation which addresses the influence of ~~the dynamically steady-state flow-compatible induced anisotropic crystal orientation patterns that develop when ice is subjected to the same stress regime for a prolonged period – sometimes termed tertiary flow. We call this the ESTAR flow relation.~~ The effect of ~~this anisotropic rheology~~ on ice flow dynamics is investigated by comparing idealised simulations using ESTAR ~~with those using the isotropic Glen flow relation, where the latter includes and Glen flow relations, where we include in the latter~~ an overall flow enhancement factor. For an idealised embayed ice shelf, the Glen flow relation overestimates velocities by up to 17% when using an enhancement factor equivalent to the maximum value prescribed ~~by ESTAR in the ESTAR relation.~~ Importantly, no single Glen enhancement factor can accurately capture the spatial variations in flow ~~over across~~ the ice shelf ~~for flow line generated by the ESTAR flow relation. For flow line~~ studies of idealised grounded flow over varying topography or variable basal friction – both scenarios dominated at depth by bed-parallel shear – the differences between simulated velocities using ESTAR and ~~the Glen flow relation vary according to~~ Glen flow relations depend on the value of the enhancement factor used to calibrate the Glen flow relation. These results demonstrate the importance of describing the ~~anisotropic rheology of deformation of anisotropic~~ ice in a physically realistic manner, and have implications for simulations of ice sheet evolution used to reconstruct paleo-ice sheet extent and predict future ice sheet contributions to sea level.

20 1 Introduction

An essential component of ~~an any~~ ice sheet model is ~~its formulation of ice rheology, which relates deformation rates to the constitutive relation (or flow relation), which connects ice deformation rates and~~ applied stresses. ~~Data from laboratory ice~~

deformation experiments can be used to define flow relations suitable for implementation in numerical ice sheet models. Previous experiments have demonstrated that under conditions of constant stress and temperature, polycrystalline ice with a statistically random distribution of crystallographic Under prolonged deformation polycrystalline ice aggregates develop material anisotropy, patterns of preferred orientations of individual crystal c -axes (fabric) initially behaves as a mechanically isotropic material (Budd and Jacka, 1989) where the rate of deformation is not sensitive to the character of the applied stresses. We use the term fabric to describe the distribution of crystallographic c -axis orientations within a polycrystalline aggregate. At the commencement of deformation, during the primary stage of creep, the initially high strain rate rapidly decreases. A minimum strain rate is reached during secondary creep (Fig. 1), which is associated with a transitory balance between strain hardening and the strain-induced activation of microstructural recovery processes. With continued strain, a tertiary stage of creep is established (typically observed at strain of $\sim 10\%$ in laboratory experiments), which is characterised by a dynamic balance between microdeformation and recovery processes, statistically steady-state anisotropic polycrystalline microstructures (e. g., crystal orientation fabric and grain size), and steady strain rates that are enhanced relative to the rate observed during secondary creep.

Tertiary creep, with the associated development of polycrystalline anisotropy driven by the microstructural response to applied stresses, is the predominant mode of ice deformation in ice sheets (Budd and Jacka, 1989). The pattern of fabric anisotropy and the tertiary strain rates both depend on the nature of the applied stresses (Fig. 1). Attaining a state of tertiary creep requires that a stable pattern of stresses acts for sufficient time to develop the compatible crystal anisotropy. We can expect this tertiary state to be common throughout the bulk of a polar ice sheet from simple considerations of the observed velocities and strain rates, provided the spatial pattern of deformation varies slowly compared to the passage of ice through that pattern. Clearly there are also some regions where tertiary flow is not expected to be achieved. We discuss applicability of this tertiary creep assumption in more detail in Sects. 3.2 and 3.3, and in discussions in Sect. 7 in light of the results of axes, which we refer to as anisotropic fabrics. There is broad agreement that deformation under stresses within polar ice sheets leads to widespread development of anisotropic fabrics (e.g., Budd and Jacka, 1989; Hudleston, 2015), through a variety of physical processes (e.g., Faria et al., 2014). The development of these anisotropic fabrics is associated with different deformation rates for different patterns of applied stresses. Laboratory deformation tests (e.g. Russell-Head and Budd, 1979; Bouchez and Duval, 1982; Jacka field evidence (e.g., Wang and Warner, 1999; Wang et al., 2002a; Treverrow et al., 2015) indicate that the idealised experiments influence of anisotropy on deformation rates is significant for polar ice sheets and should be incorporated in flow relations used in large-scale ice sheet models.

The There are complex flow relations that explicitly include material anisotropy, and models that track the evolution of crystal fabrics, as discussed briefly below, but the Glen flow relation (Glen, 1952, 1953, 1955, 1958; Nye, 1953) is the prevailing description of ice rheology used deformation in large-scale ice sheet models, the Glen flow relation (Glen, 1952, 1953, 1955, 1958; Nye, 1953) is a creep power law:-

$$\dot{\epsilon} = A(T')\tau_e^{n-1}\sigma',$$

where. It is given by the following expression

$$\dot{\epsilon} = A(T')\tau_e^{n-1}\sigma'. \quad (1)$$

Here, $\dot{\epsilon}$ is the strain rate tensor (s^{-1}), τ_e is the effective stress (Pa), proportional to the second invariant of the deviatoric stress tensor σ' , and n is a power law stress exponent (observations support a value of $n = 3$). $A(T')$ is a flow parameter ($\text{Pa}^{-n} \text{s}^{-1}$), dependent on homologous temperature T' and persistent material properties, for which various parameterisations exist based on laboratory tests and field measurements (e.g., Budd and Jacka, 1989; Cuffey and Paterson, 2010).

(e.g., Budd and Jacka, 1989; Cuffey and Paterson, 2010, p. 73). The Glen flow relation was empirically derived from secondary creep rates, determined under various conditions of constant stress and temperature, for polycrystalline ice with an initially random distribution of c -axes and assuming mechanical isotropy. While is not expected to hold for anisotropic ice (Budd et al., 2013), being empirically derived under the assumption of mechanical isotropy (Nye, 1953), which necessarily restricts the possible structure of the flow relation (Glen, 1958). Hence, while the Glen flow relation captures the observed nonlinear response of ice deformation to the magnitude of the applied stresses, it is unable to account for the mechanical anisotropy of polycrystalline ice that develops during the transition to tertiary creep (e.g., Nye, 1953; Glen, 1958; Budd et al., 2013). That is, it cannot explain the dependence of tertiary-observed dependence of steady-state strain rates on the character of the applied stress.

To account for the increased deformability associated with tertiary-steady-state creep, a common adaptation of the Glen flow relation is the inclusion of a constant flow enhancement factor, E_G ,

$$\dot{\epsilon} = E_G A(T')\tau_e^{n-1}\sigma'. \quad (2)$$

The Such a parameter is included in most large-scale ice sheet models (e.g., Saito and Abe-Ouchi, 2004; Greve, 2005; Huybrechts et al., 2007) typically to increase the rates expected in the bed-parallel shear that is important in ice sheets. However, the specification of E_G is typically ad hoc: E_G may be selected from reported experimental values (e.g., Duval, 1981; Jacka and Maccagnan, 1984; Pimienta et al., 1987; Treverrow et al., 2012), or used as a model tuning parameter. Such a parameter is included in most large-scale ice sheet models (e.g., Saito and Abe-Ouchi, 2004; Greve, 2005; Huybrechts et al., 2007; Winkelmann et al., 2011). Indeed, Greve and Blatter (2009) comment that E_G is “often introduced without explicitly mentioning anisotropy”. In any case, a value of E_G that does not vary spatially in connection with the fabric and flow configuration, will lead to an unrealistic spatial distribution of strain rates (Wang and Warner, 1999; Wang et al., 2002a; Treverrow et al., 2015). Previous studies have used anisotropic flow models or approximations to assign assigned regional values to E_G (e.g., Ma et al., 2010) that may also vary according to the prevailing stress regime.

Budd et al. (2013) recently proposed an anisotropic a flow relation based on results from laboratory ice deformation experiments involving simple shear, compression, and combinations of these. As tertiary creep rates and the These experiments reached steady-state creep rates – also referred to as tertiary flow. As these strain rates and corresponding compatible fabrics were found to vary according to depending on the relative proportions of the simple shear and compression stresses, Budd et al. (2013) defined an enhancement factor E as an anisotropic a function of the stress configuration, based on interpolating between separate, experimentally-determined enhancement factors for simple shear alone and compression alone. The laboratory experiments

were satisfactorily described by a scalar relation between stresses and strain-rates (Budd et al. (2013)), which motivated the suggestion that this might extend to general stresses. We refer to the generalised ~~form of the anisotropic~~ flow relation proposed by Budd et al. (2013) as ESTAR (Empirical ~~, Scalar, Tertiary, Anisotropic Rheology~~ Scalar Tertiary Anisotropy Regime), since it is based on ~~tertiary~~ (steady-state ~~(tertiary)~~ creep rates describing the deformation of ~~anisotropic ice~~ ice with a flow-compatible induced anisotropy and features a scalar (collinear) relationship between the strain rate and deviatoric stress tensor components. As discussed below, the ESTAR relation is a mathematically isotropic flow relation for ice with a fully developed anisotropic fabric compatible with the deformation regime. While this flow relation will not capture the all the influences of the full variety of anisotropic crystal fabrics, nor situations where the fabric and stress regime are not compatible, we suggest it should provide an improvement on the Glen flow relation.

Here, as a first step towards exploring the implications of this description of ~~tertiary creep~~ anisotropic ice in large-scale ice sheet models, we describe how to implement ~~ESTAR in large-scale ice sheet models~~ the ESTAR flow relation and apply the required changes to the Ice Sheet System Model (ISSM; Larour et al., 2012). ISSM is a thermomechanical finite element model that solves the full system of Stokes equations to describe ice flow. This will permit exploration of the ramifications of ~~ESTAR~~ the ESTAR flow relation in general ice flow situations. In ~~an initial study~~ here this initial study, we examine the effect of induced anisotropy in simple, idealised scenarios of a floating ice shelf and of grounded ice sheets, comparing ~~simulated flow fields using ESTAR with the corresponding isotropic flow modelled by the Glen flow relation~~ flow fields simulated using ESTAR and Glen flow relations. Section 2 discusses the role of anisotropic ice in polar ice sheets. Section 3 presents a brief overview of ~~anisotropic rheologies, including flow relations for ice with a polycrystalline anisotropy, focussing on~~ the experimental and theoretical basis for ~~ESTAR~~ and applicability of the ESTAR flow relation. Section ~~??~~ 4 details the implementation of ~~ESTAR~~ the ESTAR flow relation in ISSM while Sect. 5 verifies the implementation against an analytical solution. In Sect. 6, we compare simulations of ice flow with ~~ESTAR and the Glen flow relation~~ the ESTAR and Glen flow relations using a suite of idealised flow geometries, including selected experiments from the Ice Sheet Model Intercomparison Project for Higher Order Models (ISMIP-HOM; Pattyn et al., 2007). Section 7 discusses the results, and implications of the ESTAR description of the flow of ~~anisotropic ice~~ ice with a flow-induced crystallographic anisotropy. Conclusions are drawn together in Sect. 8.

25 2 ~~Anisotropic~~ Anisotropy and polar ice ~~rheology~~ sheets

In this section we outline the development of anisotropic fabrics in polycrystalline ice, including the tertiary flow regime and its connection with enhanced deformation rates and development of compatible anisotropy, and discuss the expected occurrence of anisotropy and tertiary flow conditions in polar ice sheets.

Individual ice crystals have a strong mechanical anisotropy, owing to high levels of deformability due to slip on the crystallographic basal plane, whose normal is the crystallographic c -axes. Under prolonged deformation, the microstructure of ice evolves, leading to the development of patterns of preferred c -axis orientations (crystal orientation fabric). While the direct evidence for anisotropic fabrics in polar ice sheets is limited to data from a small number of deep ice core sites, the long passage of ice through the ice sheet stress regime makes this inevitable. In the course of flow through a polar ice sheet

each parcel of polycrystalline ice is deformed by exposure to patterns of stress which usually change gradually, the most obvious being stresses dominated by vertical compression through the upper part of the ice sheet before a smooth transition to predominantly bed-parallel simple shear below.

5 As discussed by Budd and Jacka (1989) the nature of the applied stresses and the rotation with the flow produce anisotropic crystal fabrics that evolve to reflect the accumulating strain history and flow. These fabrics necessarily have a compatibility with their strain history, and if we assume that fabrics usually develop within time frames that are short compared to the rates at which the ice encounters changing stress regimes (Thorsteinsson et al., 2003) they will typically be compatible with recent strain history and by extension with the current stress regime.

10 There are exceptional locations where this concept of compatibility is likely to break down – where the stress regime experienced by the flowing ice alters rapidly. Examples include transitions from tributary glacier or sheet flow into the shear margins of ice streams or ice shelves (e.g. Thorsteinsson et al., 2003), and for deeper layers the transition from bed-parallel shear to extensional flow at ice shelf grounding lines or at the onset of ice streams. Thorsteinsson et al. (2003) also point out that temporal changes in the stress regime, such as divide migration, can provide a more abrupt change than advection of ice through a steady distribution of stresses.

15 In their review, Budd and Jacka (1989) made a further conjecture about the character of the anisotropic fabrics. Comparing evidence from an array of boreholes on Law Dome, East Antarctica (the most extensive ice coring program focussed on ice dynamics rather than paleoclimate) with laboratory studies of ice deformation, they suggested that as ice passes through the varying ice sheet stress regime, it likewise passes through a succession of “steady-state” fabrics, which they termed tertiary flow. We return to this point after a brief review of the stages of deformation observed in the accommodation to a fixed stress from a laboratory perspective.

20 Experimental observations for pure polycrystalline ice, demonstrate that an accumulated strain of $\geq 10\%$ is required for the microstructure to evolve to a state that is compatible with the flow configuration, irrespective of its initial condition (Jacka and Maccagnan, 1984; Gao and Jacka, 1987; Li and Jacka, 1998; Treverrow et al., 2012). Specifically, laboratory experiments have demonstrated that under conditions of constant stress and temperature, deformation of polycrystalline ice with an initial statistically random distribution of crystallographic *c*-axes (isotropic fabric) passes through three stages. Initially it behaves as a mechanically isotropic material (Budd and Jacka, 1989) where the rate of deformation is not sensitive to the character of the applied stresses. At the commencement of deformation, during the primary stage of creep, the initially high strain rate rapidly decreases. A minimum strain rate is reached during secondary creep (Fig. 1). With continued strain, a tertiary stage of creep is established (typically observed at strain of $\sim 10\%$ in under laboratory conditions) with steady strain rates that are enhanced relative to the rate observed during secondary creep, and characterised by the development of statistically steady-state anisotropic microstructures that are associated with the stress regime. We describe this as tertiary anisotropy. An important feature of the experiments is that for the same stress magnitude the enhanced tertiary deformation rates under compression alone or simple shear alone are different (Budd and Jacka, 1989; Treverrow et al., 2012). Laboratory experiments also indicate that attainment of enhanced deformation rates precedes the full development of anisotropic fabrics (Jacka and Maccagnan, 1984), suggesting that strain rate does not alter much once the most obstructive grains have been removed by fabric development.

There are a variety of microdeformation and recovery processes that lead to the development of anisotropic fabrics (e.g. Faria et al., 2014) however, there is not a consensus on how the activity of specific processes may vary according to temperature and/or stress. Observations from ice cores can provide guidance on the temperature domain over which laboratory observations remain indicative of in-situ behaviour. For the A001 ice core drilled at the summit of Law Dome, East Antarctica, a distinct small circle girdle (cone-type) fabric (the compression-compatible form) is observed at a depth of 318 m (Fig. 3a Budd and Jacka, 1989), where the total accumulated strain is $\sim 30\%$, the temperature is $\sim -22^\circ\text{C}$, and the in-situ flow regime is compression dominated with approximately radial symmetry in the transverse rates. Since the fabric is already well developed at this point, the actual strain required to achieve tertiary creep was probably less. Similar compression-compatible fabrics have been observed in the laboratory at higher temperatures and stresses (e.g. Jacka and Maccagnan, 1984; Treverrow et al., 2012). Accordingly, these observations suggest a conservative temperature limit of $\sim -22^\circ\text{C}$ for extrapolating laboratory observations of fully developed tertiary creep down to in-situ conditions.

Information about the effects of anisotropy on in-situ deformation rates in polar ice sheets is limited. Analyses of the shear strain rate profiles inferred from bore hole inclination measurements on Law Dome (Russell-Head and Budd, 1979; Wang and Warner, 1999) enhancement in deformation rates correlated with the stress regime consistent with tertiary flow, and fabrics that match the expectations of the laboratory experiments (Donoghue and Jacka, 2009; Treverrow et al., 2016).

While the relevant temperature regime and the amount of strain that needs to be accumulated remains uncertain, tertiary creep, with the associated development of polycrystalline anisotropy, may be common in polar ice sheets, particularly in regions controlling the large scale dynamics, as discussed further in Sect. 3.1. This has the potential to provide a relatively simple description of the deformation properties of this anisotropic ice, since the stress regime becomes a guide to the enhanced flow, and motivates this study to incorporate an empirical tertiary flow relation into large scale ice sheet modelling, as discussed in the next section.

3 Constitutive relations for anisotropic polycrystalline ice

A range of ~~ice rheologies~~ constitutive relations have been proposed to account for polycrystalline anisotropy. They can be broadly grouped in two categories (Marshall, 2005): (1) those defined at the individual ice crystal scale, where the effects of crystallographic anisotropy are parameterised based on specific properties of individual crystals, and (2) those ~~that describe anisotropic aspects of deformation empirically: either based on regional expectations about local crystallographic microstructure, or~~ connected with the present work that describe the deformation of ice with flow-compatible anisotropy, through an empirical function of the stress configuration. In this section, we briefly review these two approaches, and the underlying experimental and modelling basis for ~~ESTAR~~ the ESTAR flow relation. We then outline the expected domain where the ESTAR flow relation might apply in polar ice sheets. Lastly, we distinguish between anisotropic constitutive relations, and constitutive relations for ice with a compatible, flow-induced anisotropy. In what follows, we distinguish between the Glen enhancement factor E_G and the ESTAR enhancement factor $E(\lambda_S)$, which is a function of compression deviatoric and simple

shear stresses, parameterised by the shear fraction λ_S . Where necessary, we denote a more general enhancement factor, i.e., with unspecified form, as E .

3.1 Microstructure approaches

Experiments on single crystals of ice demonstrate that deformation occurs predominantly by slip on the crystallographic basal
5 plane (perpendicular to the c -axis), with the yield stress being geometrically related to the magnitude of the applied stress resolved onto the basal plane (Trickett et al., 2000) according to Schmid's Law (Schmid and Boas, 1950). ~~This observation~~In the formulation of the Glen flow relation for polycrystalline ice the assumed isotropic distribution of c -axes results in indifference to material rotations (relative to applied stresses) and an isotropic expression. The underlying anisotropic deformation properties of individual crystals, in conjunction with the development of crystallographic preferred orientations during deformation of
10 polycrystalline ice to high strains (e.g. Russell-Head and Budd, 1979; Jacka and Maccagnan, 1984; Pimienta et al., 1987; Morgan et al., 1998; DiPrinzio et al., 2005; Durand et al., 2009; Budd et al., 2013; Montagnat et al., 2014), has driven the development of ~~rheological descriptions~~constitutive relations in which the connection between deviatoric stresses and resulting strain-rates is regarded as an intrinsic material property determined by the effects of microstructure on bulk deformation processes, (e.g. Lile, 1978; Lliboutry, 1993; Azuma and Goto-Azuma, 1996; Staroszczyk and Gagliardini, 1999; Thorsteinsson,
15 2001; Gödert, 2003; Gillet-Chaulet et al., 2005; Pettit et al., 2007; Placidi et al., 2010). See also the review by Gagliardini et al. (2009). ~~In broad terms, the anisotropic nature of these rheological descriptions is derived from the~~These constitutive relations describe polycrystalline anisotropy through the geometric relationship between the crystallographic c -axes and the stresses driving deformation, with the role of misorientation relationships between nearest neighbour grains explicitly considered in some cases.

20 The complexity of ~~numerical~~resulting flow relations varies according to the extent to which a physically realistic description of microdeformation and recovery processes, or a parameterisation of these, enters into the relationship between strain rates and the stresses driving deformation. Many of these ~~rheological~~constitutive models are more complicated than a collinear flow relation and involve a tensor coupling in place of Eq. 2. A further consideration is the quantitative description of fabric that is used in flow relations. Those incorporating a discrete ~~, c -axis vector-based~~vector-based description of fabric
25 ~~(e.g. Lile, 1978; van der Veen and Whillans, 1994; Azuma and Goto-Azuma, 1996; Thorsteinsson, 2002)~~are only appropriate based on c -axes (e.g. Lile, 1978; van der Veen and Whillans, 1994; Azuma and Goto-Azuma, 1996; Thorsteinsson, 2002) are appropriate only for highly localised studies and are incompatible with large-scale ice sheet modelling. Flow relations based on a continuous description of fabric, e.g., a parameterised orientation distribution function (ODF) or c -axis orientation tensor are also possible (e.g. Staroszczyk and Gagliardini, 1999; Gödert, 2003; Gillet-Chaulet et al., 2005; Pettit et al., 2007; Placidi
30 et al., 2010). A central tenet of these microstructure-based constitutive relations is that they require the specific input of the anisotropic character of the material being deformed. They describe the instantaneous deformational response of any sample of ice to any pattern of applied stresses. In this regard they can be defined as anisotropic flow relations, whether they involve a tensor or a scalar connection between stresses and strain-rates (Faria, 2008).

Including any fabric-based ~~rheological description in~~ description of material anisotropy in the flow relation for an ice sheet model requires ~~a separate either a prescription of anisotropy or an additional~~ set of equations governing the fabric evolution. A complication of such an approach is the computational overhead and uncertainty associated with defining the spatial distribution of fabric within ice sheets, which is poorly constrained by observations. ~~Furthermore, for simplicity~~ Sometimes, as a
5 simplification, restricted forms of the ODF or orientation tensor are specified, which may not adequately describe all fabrics likely to be encountered in an ice sheet. ~~As such~~ To date, flow relations utilising a fabric description that relies on fabric evolution equations or that is imposed as a function of location within the ice sheet are currently restricted to regional simulations (e.g., Seddik et al., 2011; Martín and Gudmundsson, 2012; Zwinger et al., 2014).

3.2 Empirical approaches to tertiary flow

10 ~~A second approach~~ As indicated in Sect. 2 a flow relation applicable to the tertiary regime may provide a useful description of deformation, capturing important aspects of the flow of anisotropic ice in polar ice sheets.

An empirical approach to the deformation properties of ice with a tertiary polycrystalline anisotropy has developed, comprising experimental and observational ~~approaches~~ studies (Li et al., 1996; Wang et al., 2002a, b), modelling (Wang and Warner, 1998, 1999; Hulbe et al., 2003; Wang et al., 2003, 2004; Breuer et al., 2006; Wang et al., 2012), and theoretical
15 ~~studies (Warner et al., 1999)~~. This empirical approach has focussed on the development and assessment of ~~an anisotropic~~ a flow relation for polycrystalline ice in which the nature of the circumstance where the crystal fabric and the ~~magnitude of strain rate enhancement, E , are both regarded as flow properties are both~~ determined by the stress regime. ~~This assumption is supported by experimental observations for pure polycrystalline ice, which demonstrate that an accumulated strain of $\sim 10\%$ is required for the microstructure to evolve to a state that is compatible with the flow configuration, irrespective of its~~
20 ~~initial condition (Jaeka and Maccagnan, 1984; Gao and Jaeka, 1987; Li and Jaeka, 1998; Treverrow et al., 2012)~~. Specifically, this approach regards the fabric and the enhancement in tertiary flow as determined by the; specifically, the relative proportions of the simple shear and normal deviatoric stresses. For such flow relations, it is typically assumed that the spatial variation in dynamic conditions (e.g., flow configuration and temperature) ~~only occur~~ occur only gradually in an ice sheet, so that the microstructure evolves to maintain compatibility with these conditions. Through most of an ice sheet we expect that the rate
25 of microstructural evolution generally exceeds the rate at which the flow configuration varies, and that the distances travelled by a parcel of ice during the time taken to develop a compatible fabric are typically small compared to the relevant ice sheet spatial scales.

~~The anisotropic~~ A flow line model by Wang and Warner (1999) implemented an empirical enhancement function based on the stress regime, using a compression fraction, $\lambda_C = \sqrt{1 - \lambda_S^2}$, and an earlier parameterisation of tertiary enhancement, $E(\lambda_C)$, from Li et al. (1996). That study of a flow line on Law Dome, East Antarctica, showed how an enhancement function improved agreement with observations of shear strain rate profiles from borehole inclination measurements, and displayed
30 correlations with ice core crystal fabrics. Wang et al. (2002a) demonstrated that vertical variation of enhancement was required to match the shear strain rate profile from the Law Dome Summit South (DSS) borehole, and showed its correlation to stress configuration, and the connection with crystal fabric anisotropy.

The generalised tertiary flow relation proposed by Budd et al. (2013) represents a continuation of this strand. ~~They~~ While more complicated parameterisations were also explored, Budd et al. (2013) found that a scalar anisotropic flow relation, i.e., one maintaining the collinear relationship between the components of $\dot{\epsilon}$ and σ' (τ_e is a scalar function of σ' , with a functional dependence on both the second invariant of σ') provides and the fraction of the deformation that was simple shear, provided a good fit to laboratory data from for tertiary flow in combined compression and shear experiments. Such a scalar anisotropic rheology also simplifies the requirements for implementation within ice sheet models that are already compatible with the (scalar) Glen rheological description. Budd et al. (2013) Given this scalar character, they proposed what we term ESTAR the ESTAR flow relation as a suitable candidate scalar anisotropic rheology generalised to flow relation for arbitrary stress configurations (i.e., not restricted in its application, extrapolating from its applicability to the limited set of experimental stress configurations described in Li et al. (1996) and Budd et al. (2013)). A scalar relation also simplifies the requirements for implementation within ice sheet models that currently use the Glen flow relation. A simplified version of ESTAR, called ESTAR-MFL (MFL the ESTAR flow relation, called ESTAR-MFR (MFR: Minimal Flow Law Relation), has also been incorporated into the ice sheet model SICOPOLIS (SIMulation COde for POLythermal Ice Sheets, <http://www.sicopolis.net>; Greve and Blatter, 2009, 2016).

There are of course zones within an ice sheet where the assumption of compatible tertiary flow will not apply; however, we note that these zones will be restricted in their extent. We contend that ESTAR will apply to the vast majority of the dynamically active regions of an ice sheet, in particular the zones where creep deformation makes a significant contribution to the overall flow. Specific zones where the assumption of tertiary creep may be inappropriate can be summarised as those where fabric has not yet evolved compatibility with the flow, where there is a rapid transition in the flow configuration, or where creep deformation makes only a minor contribution to the overall dynamics.

For example, in very cold ice in a low stress setting, such as the uppermost layers of the polar ice sheets, the time required to accumulate the strain necessary to develop a compatible fabric may lead to a near-surface zone in which the assumption of tertiary creep is not valid. Since the development of anisotropic fabrics provides an indication of the existence of tertiary flow, their observation at modest depths, (e.g., $\lesssim 100 - 200$ m; Morgan et al., 1997; DiPrinzio et al., 2005; Treverrow et al., 2016) allows estimation of the maximum extent of the zone where tertiary creep is not occurring. The observation within polar firn of microdeformation processes that are necessary for the development of fabric throughout ice sheets (e.g. Kipfstuhl et al., 2009; Faria et al., 2012) that it may be appropriate to even further restrict the extent of the near-surface zone for which the assumption of tertiary creep is not valid. Additionally, the nonlinear nature of polycrystalline ice rheology leads to very high viscosities in low temperature and stress environments, so that incorrectly estimating deformation rates due to the assumption of tertiary flow in such regions may be of limited importance to simulations of ice sheet evolution.

Regions where rapid transitions in dynamic conditions can lead to abrupt changes in the pattern of applied stresses and a potential breakdown in tertiary flow compatibility include ice shelf grounding zones and other locations where basal traction is lost or abruptly changes, e.g., where ice flows over a subglacial lake, or with the onset of basal sliding in ice streams. The convergence zones where tributary glaciers or ice streams merge with a larger flow unit at a high angle may also lead to a transition in dynamic conditions that is problematic for the assumption of tertiary compatibility. Of course the more highly

dynamic the evolving flow regime, the more rapidly a new compatible anisotropy will be established, so that the spatial interval where the flow relations are inapplicable may be limited. While there is little guidance on how to extend empirical flow relations to parametrise ice rheology in these transition regions, we note that similar difficulties exist for a Glen-type flow relation, which unlike ESTAR does not have the benefit of being able to correctly describe anisotropic enhancement throughout the remainder of the ice sheet.

3.3 Empirical scalar tertiary anisotropic rheology (ESTAR)

3.3 Empirical Scalar Tertiary Anisotropy Regime (ESTAR) flow relation

Here, we summarise the anisotropic rheology Here, we summarise the generalised constitutive relation for ice in tertiary flow (the ESTAR flow relation) proposed by Budd et al. (2013)—ESTAR—that we are implementing. We are implementing this in ISSM as an alternative to the Glen flow relation ,to provide a relation as the ESTAR flow relation is more applicable to the tertiary creep of anisotropic polycrystalline ice typical of ice sheets and glaciers. ESTAR in ice sheets. The ESTAR flow relation is a scalar power law formulation based on tertiary creep rates measured in laboratory ice deformation experiments under various combinations of simple shear and compression that has been generalised to arbitrary stress configurations. Recasting Eqs. 62 and 63 of Budd et al. (2013) to more closely resemble Eq. 2, ESTAR is given by the following expression:-

$$\dot{\epsilon} = E(\lambda_S) A(T') \tau_e^2 \sigma'.$$

Assuming $n = 3$ in Eq. 2, Eq. 3 only differs from the Glen flow relation by the form of the functional enhancement factor $E(\lambda_S)$, which explicitly depends on the nature of the applied stresses via the shear fraction, λ_S , and could be regarded as providing a variable enhancement function for the Glen relation that incorporates the effect of anisotropy. We note in passing that in contrast to ISSM, flow relations in Budd et al. (2013) are couched in terms of the octahedral shear stress, $\tau_o = \sqrt{2/3} \tau_e$, which provides a more physically meaningful scalar measure of the overall stress magnitude than τ_e (Jaeger, 1969) .

$E(\lambda_S)$ in Eq. 3 is defined as

$$E(\lambda_S) = E_C + (E_S - E_C) \lambda_S^2,$$

where E_C The main features of Budd et al. (2013) and E_S are the enhancement factors above the minimum or secondary deformation rate of isotropic ice under compression alone or simple shear alone, respectively. The shear fraction λ_S in Eq. 4 is a non-dimensional variable taking values in $[0, 1]$, which characterises the contribution of simple shear (τ') to the effective stress (τ_e)

$$\lambda_S = \frac{\|\tau'\|}{\tau_e}.$$

The essence of Budd et al. (2013) and ESTAR is the ESTAR flow relation are the observation that tertiary strain rates depend on the nature of the applied stresses, and the identification of the shear fraction λ_S is proportion of the overall deformation stress that can be regarded as simple shear as the appropriate variable to characterise that pattern dependency. Accordingly,

determining the ~~portion of the overall deformation stress that can be regarded as simple shear~~ shear fraction, λ_S , is the main ~~ingredient in implementing ESTAR~~ task in implementing the ESTAR flow relation. This involves the identification of a particular local plane – the local non-rotating shear plane – and the determination of the shear acting on that plane, τ' , as the measure of simple shear. As ~~discussed in Budd et al. (2013)~~, the indicated in Sect. 4 below Budd et al. (2013) also prescribed
5 a further projection to remove any component of τ' parallel to the deformational vorticity. The importance of moving beyond strain rates to consider other aspects of flow – the ‘movement picture’ – has been recognised since at least the 1970s (e.g., Budd, 1972; Kamb, 1973; Duval, 1981) (e.g., Budd, 1972; Kamb, 1973; Duval, 1981; Budd et al., 2013). Duval (1981) identified the plane normal to the velocity gradient in a simple shear regime as the ‘permanent shear plane’ and discussed its role in the evolution of crystal fabrics. Budd et al. (2013) proposed a local definition for this local plane in an arbitrary flow as
10 the plane containing the velocity vector and the vorticity vector associated solely with deformation.

Recasting Eqs. 62 and 63 of Budd et al. (2013) to more closely resemble Eq. 2, the ESTAR flow relation is given by the following expression:

$$\dot{\epsilon} = E(\lambda_S) A(T') \tau_e^2 \sigma'. \quad (3)$$

Assuming $n = 3$ in Eq. 2, Eq. 3 differs from the Glen flow relation only by the form of the functional enhancement factor $E(\lambda_S)$, which could be regarded as providing a variable enhancement function for the Glen relation that incorporates the effect of flow-induced fabric anisotropy. $E(\lambda_S)$ in Eq. 3 is defined as

$$E(\lambda_S) = E_C + (E_S - E_C) \lambda_S^2. \quad (4)$$

Here, E_C and the velocity vector. As discussed below they also prescribed a further projection to remove any component of τ' parallel to the deformational vorticity. The E_S are the enhancement factors above the minimum or secondary deformation rate of isotropic ice under compression alone or simple shear alone, respectively, and λ_S is the shear fraction, which characterises the contribution of simple shear to the effective stress. The shear fraction λ_S can then be written as

$$\lambda_S = \frac{\|\tau'\|}{\tau_e}. \quad (5)$$

The collinear nature of ESTAR the ESTAR flow relation (Eq. 3) allows λ_S to be written in terms of the corresponding strain rates, which is more convenient for Stokes flow modelling, as

$$\lambda_S = \frac{\dot{\epsilon}'}{\dot{\epsilon}_e}, \quad (6)$$

where $\dot{\epsilon}'$ is the magnitude of the shear strain rate on the locally non-rotating shear plane, as defined in Eq. 7 below. In compression-alone scenarios, including three-dimensional uniaxial compression and two-dimensional plane compression and extension, $\lambda_S = 0$, so that $E(\lambda_S) = E_C$. Similarly, for simple shear alone, $\lambda_S = 1$ and $E(\lambda_S) = E_S$.

Analysis of tertiary creep rates for experiments conducted in simple shear-alone and compression-alone suggests that a
30 suitable ratio of E_S to E_C for ice sheets is $\sim 8/3$ (Trevorrow et al., 2012). The same study also suggests that $E \propto \sqrt{\tau_e}$

for tertiary creep rates determined over a range of stress magnitudes. A flow relation incorporating such a stress dependent enhancement could be achieved by employing a creep power-law stress exponent of $n = 3.5$, rather than the more commonly used $n = 3$, assuming both E_S and E_C are described by functions of $\sqrt{\tau_e}$. For simplicity, we have excluded the apparent stress dependence of E_S and E_C in our initial implementation of ~~ESTAR~~ the ESTAR flow relation in ISSM since further
5 work is required to verify the stress dependence of E_S and E_C experimentally for complex, combined stress configurations. Accordingly, we use scalar enhancement factors of $E_S = 8$ and $E_C = 3$ for the idealised scenarios examined in this study. These values may be at the higher end of the anticipated range in E_S and E_C for an ice sheet (see e.g., Russell-Head and Budd, 1979). However, the strength of anisotropy and its influence on ice dynamics in comparison to the enhanced Glen flow relation depends on the ratio E_S/E_C and its spatial variation, i.e., the dynamically controlled distribution of $E(\lambda_S)$.

10 If the enhancement parameters are selected so that $E_C = E_S = E_G$, where E_G is the Glen enhancement factor, ~~ESTAR becomes isotropic and equivalent~~ the ESTAR flow relation loses its dependence on the stress regime, reducing to the Glen flow relation since $E(\lambda_S) \equiv E_G$. However, the viscous creep behaviour of polycrystalline ice is highly anisotropic and regional variations in the relative proportions of shear and normal strain rates, which are driven by variations in the distribution of the stresses responsible for deformation, mean that spatial contrasts in anisotropy are common and widespread in ice sheets. For
15 this reason, a spatially varying enhancement factor is required for ice sheet modelling (e.g., Morgan et al., 1998; Wang and Warner, 1999; Wang et al., 2002a).

Comparisons of simulations of ice sheet dynamics using ~~ESTAR and the Glen flow relation~~ the ESTAR and Glen flow relations will be influenced by: the choice of the Glen enhancement parameter, E_G ; the ESTAR parameters E_C and E_S ; and the spatial distribution of λ_S . The most significant differences between ~~Glen and ESTAR-based simulations are expected~~
20 simulations using Glen and ESTAR flow relations are expected to arise where there are regional contrasts in λ_S . Specific regions where these conditions are likely to arise include: the progression with increasing depth in the ice sheet from a regime of normal stresses to one dominated by bed parallel shear; the contrasts between lateral margins of embayed ice shelves and ice streams and their central flows; and where there is significant relief in the bedrock topography.

A caveat is that as stated earlier, for ~~ESTAR the assumptions of the ESTAR flow relation to hold, the assumption of the~~
25 tertiary state (i.e., crystallography and deformation rates being compatible with the instantaneous stress/deformation regime) requires that this does not change too rapidly along the flow. That is to say, for a compatible (tertiary) anisotropy to be present, the present deformation regime needs to be a suitable indicator of the recent strain history of the flowing ice.

4 **Implementation of ESTAR**

~~The magnitude of the~~

30 **3.1 Domain of applicability of tertiary creep and the ESTAR flow relation**

As discussed in Sect. 2 two conditions need to be satisfied for the applicability of the tertiary creep concept and the ESTAR flow relation – activation of the appropriate microstructural processes to generate steady-state fabrics, and sufficiently gradual

changes in the stress regime experienced by the flowing ice to permit a quasi-steady transition in the fabric and corresponding deformation rate as controlled by the shear fraction λ_S .

5 Within an ice sheet there will be zones where the assumption of compatible tertiary flow will not apply; however, these zones will be restricted in extent (Thorsteinsson et al., 2003). We contend that the ESTAR flow relation will apply to the majority of the dynamically active regions of an ice sheet, in particular those zones where creep deformation makes a significant contribution to the overall flow. Specific zones where the assumption of tertiary creep may be inappropriate can be summarised as those where the fabric has not yet evolved compatibility with the flow, where there is a rapid transition in the flow configuration, or where creep deformation makes only a minor contribution to the overall dynamics.

10 Regions where rapid transitions in dynamic conditions can lead to abrupt changes in the pattern of applied stresses and a potential breakdown in tertiary flow compatibility include ice shelf grounding zones and other locations where basal traction is lost or abruptly changes, e.g., where ice flows over a subglacial lake, or with the onset of basal sliding in ice streams. The convergence zones where tributary glaciers or ice streams merge with a larger flow unit at a high angle (Thorsteinsson et al., 2003) may also lead to a transition in dynamic conditions that is problematic for the assumption of tertiary compatibility. Of course the more highly dynamic the evolving flow regime, the more rapidly a new compatible anisotropy will be established, so that the spatial interval where the flow relations are inapplicable may be limited. The effect of these localised encounters of stresses with incompatible fabrics on the overall flow is unclear; however, we note that similar difficulties exist for a Glen-type flow relation, which unlike the ESTAR flow relation does not have the benefit of being able to correctly describe enhanced flow rates throughout the remainder of the ice sheet.

20 Under the very cold and low stress conditions occurring in the uppermost layers of the polar ice sheets, particularly towards the interior at high elevations, any increase in the accumulated strain necessary to develop a compatible fabric may lead to a near-surface zone in which the assumption of tertiary creep is not valid. Since the development of anisotropic fabrics provides an indication of the existence of, or the approach towards tertiary flow, the observation of evolving anisotropic fabrics at modest depths, (e.g., $\sim 100 - 200$ m; DiPrinzio et al., 2005; Montagnat et al., 2014; Treverrow et al., 2016) allows the maximum extent of the zone where tertiary creep is not occurring to be estimated. Because the nonlinear nature of polycrystalline ice deformation rates leads to very high viscosities in low temperature and stress environments, incorrectly estimating deformation rates due to the assumption of tertiary flow in such regions may be of limited importance to simulations of ice sheet evolution.

3.2 The semantics of anisotropy

30 We conclude this section with some remarks about the seeming paradox of using an isotropic constitutive relation to describe the deformation of ice that has an anisotropic pattern of c -axis orientations.

Anisotropy in broad terms describes differences in physical systems associated with different directions. The various flow relations in Budd et al. (2013) involve a specific direction, namely the normal to the non-rotating shear plane that is determined by the combination of the stress regime and the flow, and also connect the strain rates with the character of the stress regime through the shear fraction λ_S .

In materials science, anisotropy is used to refer to material properties which have different values when measured along different directions. Indeed, the term is often introduced (e.g., Kocks et al., 1998) as the opposite to isotropy or indifference to rotations. Polycrystalline ice with a c -axis distribution that exhibits certain preferred directions clearly displays anisotropy, though the manifestation of this physically discernible feature in deformational properties requires demonstration.

5 Microstructural approaches to ice deformation, such as those discussed in Sect. 3.1 above, typically aim to describe the prompt response (ignoring transient primary creep) of ice with any crystal fabric to an arbitrary arrangement of applied stresses, where the emphasis on promptness covers ignoring any resultant fabric evolution. In this context it is variation in the response to applied stresses under rotations of the anisotropic material relative to the stress distribution that could be said to characterise an anisotropic flow relation.

10 In contrast, the applicability of the flow relation we are implementing from Budd et al. (2013) is limited to ice undergoing tertiary flow, i.e., ice with an anisotropic crystal fabric induced by prolonged deformation under the same stress regime. Indeed, the directional sense of anisotropy of the fabric, its character and the resultant mechanical properties, are all characterised by the nature of the stress regime. This is not a situation amenable to considering arbitrary rotations of a material element relative to the stresses. Accordingly, as presented completely in terms of the stresses, it is an isotropic flow relation, for material with
15 a flow-compatible induced anisotropy.

The general flow relation constructed by Glen (1958) was empirically formulated on the basis of isotropy, involving only the tensors of strain-rates and deviatoric stresses, and their scalar invariants. In the most general expression provided, (Eq. 4 of Glen, 1958) the flow relation was not collinear, and by including possible dependence on the cubic invariant of the stress tensor it also contained a measure of the character of the pattern of stresses as well as the magnitude (given by the second invariant).

20 Indeed, consideration of a possible dependence on the third (cubic) invariant of σ' as an explanation of the dependence of tertiary flow rates on different stress regimes is a recurrent suggestion (e.g., Baker, 1987; Morland, 2007).

As Faria (2008) points out in discussing the CAFFE flow relation, this is a different issue from whether the flow relation involves a rank-four tensor connecting strain rates and deviatoric stresses. The CAFFE and ESTAR flow relations are both scalar (collinear) relations between deviatoric stresses and strain rates, yet only the CAFFE flow relation, whose “deformability”
25 parameter involves both stresses and the anisotropic crystal orientations is an anisotropic constitutive relation in the sense discussed above.

4 Implementation of the ESTAR flow relation

The magnitude of the shear strain rate defined on the local non-rotating shear plane, $\dot{\epsilon}'$ for Eq. 6, is central to the formulation of **ESTAR** the ESTAR flow relation (Eqs. 3-4). The full prescription, following Budd et al. (2013), involves the expression

$$30 \quad \dot{\epsilon}' = \|\dot{\epsilon} \cdot \mathbf{n} - (\mathbf{n} \cdot (\dot{\epsilon} \cdot \mathbf{n})) \mathbf{n} - (\hat{\omega}_D \cdot (\dot{\epsilon} \cdot \mathbf{n})) \hat{\omega}_D\|, \quad (7)$$

where: \mathbf{n} is the unit normal to the non-rotating shear plane, $\hat{\omega}_D$ is the unit vector parallel to that part of the vorticity that is associated solely with deformation (ω_D), and $\dot{\epsilon}$ is the strain rate tensor. The unit normal to the non-rotating shear plane, \mathbf{n} , is

defined as the normalised cross product of the velocity and the deformational vorticity

$$\mathbf{n} = \frac{\mathbf{v} \times \boldsymbol{\omega}_D}{\|\mathbf{v} \times \boldsymbol{\omega}_D\|}. \quad (8)$$

The last projection term in Eq. 7 was proposed in Budd et al. (2013) to prevent any shear component parallel to the deformational vorticity from contributing to the measure of simple shear.

5 The vorticity of a flow, whether viewed as the anti-symmetrised part of the velocity gradient tensor or as the usual vector $\boldsymbol{\omega} = \nabla \times \mathbf{v}$, contains motions associated with both deformation and local rigid-body rotation. The locally non-rotating shear plane is intended to be rotating with any rigid rotation portion of the flow field, so it is only vorticity associated with the deformation process that is relevant to determining the shear fraction. Accordingly we formally decompose vorticity into deformational and rotational parts:

$$10 \quad \boldsymbol{\omega} = \nabla \times \mathbf{v} = \boldsymbol{\omega}_D + \boldsymbol{\omega}_R. \quad (9)$$

For the present implementation it is convenient to decompose the vorticity further, into vectors perpendicular and parallel to the velocity direction as follows:

$$\boldsymbol{\omega} = \boldsymbol{\omega}_D^\perp + \boldsymbol{\omega}_R^\perp + \boldsymbol{\omega}_D^\parallel + \boldsymbol{\omega}_R^\parallel. \quad (10)$$

From Eq. 8, only the perpendicular projection $\boldsymbol{\omega}_D^\perp$ of the deformational vorticity is relevant in determining the direction of the normal to the non-rotating shear plane. This is fortunate since $\boldsymbol{\omega}_R^\perp$ the perpendicular projection of the rotational vorticity can be calculated directly for steady flow from the flow speed and the curvature of the local [flowline/streamline](#), and is oriented along the [bi-normal to the flow-line](#) [binormal \(the unit vector orthogonal to both the tangent vector and the normal vector\) to the streamline](#). The decomposition of the component of vorticity parallel to the flow direction, conventionally termed swirling motion, into deformational and rotational pieces is not so straightforward, but we can use the following expression, which can be calculated using variables available within an individual element of ISSM to generate a vector suitable for computing \mathbf{n} :

$$20 \quad \tilde{\boldsymbol{\omega}}_D = \nabla \times \mathbf{v} - \frac{2\mathbf{v} \times ((\mathbf{v} \cdot \nabla)\mathbf{v})}{\|\mathbf{v}\|^2}. \quad (11)$$

This vector contains the correct perpendicular component $\boldsymbol{\omega}_D^\perp$ to compute \mathbf{n} using Eq. 8, but contains all of $\boldsymbol{\omega}_D^\parallel + \boldsymbol{\omega}_R^\parallel$. We can obviously also project out the component parallel to velocity to find

$$\boldsymbol{\omega}_D^\perp = \tilde{\boldsymbol{\omega}}_D - (\mathbf{v} \cdot \tilde{\boldsymbol{\omega}}_D) \frac{\mathbf{v}}{\|\mathbf{v}\|^2}. \quad (12)$$

25 In the present implementation of [ESTAR](#) [the ESTAR flow relation](#), we assume that swirling effects are small for flows with the relevant spatial scales, aspect ratios etc., which can be verified from the modelled flow-fields in our test cases, and hence $\boldsymbol{\omega}_D^\parallel$ is also expected to be small. We use the unit vector corresponding to $\boldsymbol{\omega}_D^\perp$ (i.e., $\hat{\boldsymbol{\omega}}_D$) in Eq. 7 for our computation of $\dot{\epsilon}'$. This corresponds to extracting the component of the shear resolved on the non-rotating shear plane which is parallel to the velocity direction, which could be regarded as an alternative generalisation for the simple shear to that proposed by Budd et al. (2013).

No approximation is involved for flows that are exactly two dimensional in character, since vorticity is always orthogonal to velocity in such situations.

The ~~ESTAR~~[description of the ESTAR flow relation](#) above is implemented in ISSM for the full-Stokes (~~FS~~) model of flow. We also extended the implementation ~~of ESTAR~~ to ISSM versions of the higher-order (~~HO~~) three-dimensional model of Blatter (1995) and Pattyn (2003), and the shallow-shelf approximation (SSA) of MacAyeal (1989). The ~~HO~~[higher-order](#) model is derived from the ~~FS~~[full-Stokes](#) model by assuming that horizontal gradients in the vertical velocities are negligible ($\partial v_z / \partial x \ll \partial v_x / \partial z$ and $\partial v_z / \partial y \ll \partial v_y / \partial z$ ~~$\partial v_z / \partial x = \partial v_z / \partial y = 0$~~) compared with vertical gradients in the horizontal velocities [when computing vertical shear](#), and longitudinal derivatives of vertical shear stress (bridging effects van der Veen and Whillans, 1989) are ignored. The ~~HO~~[higher-order](#) vertical velocities are recovered directly through incompressibility. Extending on the ~~HO~~[higher-order](#) model assumptions, for the SSA model, vertical shear is assumed to be negligible ($\dot{\epsilon}_{xz} = \dot{\epsilon}_{yz} = 0$). For both the ~~HO~~[higher-order](#) and SSA models, the approximations will affect calculations of the total vorticity and hence the magnitude of the shear strain rate on the non-rotating shear plane (Eq. 7) and λ_S (Eq. 6).

5 Analytical verification

We perform convergence tests in order to verify the implementation of ~~ESTAR~~[the ESTAR flow relation](#) within the ISSM ~~FS~~[and HO](#) ~~full-Stokes and higher-order~~ models. The objective of these tests is to compare the model results to analytical solutions for different mesh resolutions. As the mesh becomes finer, the error between the model and the analytical solution (i.e., $\sqrt{\int_{\Omega} (X - X_a)^2 / \int_{\Omega} X_a^2}$, for model solution X , analytical solution X_a , and domain Ω) should decrease, with a cubic dependence on resolution for ~~FS~~[full-Stokes](#) (quadratic for ice pressure) when using Taylor-Hood finite elements, and a quadratic dependence for ~~HO~~[higher-order](#) using $P1 \times P1$ finite elements (e.g., Ern and Guermond, 2004).

We designed our analytical solutions by considering a three-dimensional, grounded, isothermal ice slab of unit dimension lying on a flat bed topography, with cartesian coordinates (x, y, z) , where z is vertically upward and where there is no gravitational force. The ~~FS~~[full-Stokes](#) three-dimensional velocity field is given by

$$v_x(x, y, z) = 3z, \tag{13}$$

$$v_y(x, y, z) = 2x + y, \tag{14}$$

$$v_z(x, y, z) = -z, \tag{15}$$

and the ~~HO~~[higher-order](#) velocity field by

$$v_x(x, y, z) = x^2, \tag{16}$$

$$v_y(x, y, z) = 3z + y. \tag{17}$$

In the case of the ~~HO~~[higher-order](#) model, $v_z(x, y, z)$ is recovered by incompressibility. For both ~~FS~~[and HO](#) ~~full-Stokes~~[and higher-order](#) models, we use ~~ESTAR~~ shear and compression enhancement factors of $E_S = 3$ and $E_C = 1$, and the flow parameter $A(T') = 2/3 \text{ Pa}^{-3} \text{ s}^{-1}$. The open source mathematics software system SageMath (<http://www.sagemath.org/>) is

used to calculate analytical solutions for the force balance equations based on the above velocity fields:

$$f_x(x, y, z) = - \left(\frac{\partial \sigma'_{xx}}{\partial x} + \frac{\partial \sigma_{xy}}{\partial y} + \frac{\partial \sigma_{xz}}{\partial z} \right), \quad (18)$$

$$f_y(x, y, z) = - \left(\frac{\partial \sigma_{xy}}{\partial x} + \frac{\partial \sigma'_{yy}}{\partial y} + \frac{\partial \sigma_{yz}}{\partial z} \right), \quad (19)$$

$$f_z(x, y, z) = - \left(\frac{\partial \sigma_{xz}}{\partial x} + \frac{\partial \sigma_{yz}}{\partial y} + \frac{\partial \sigma'_{zz}}{\partial z} \right). \quad (20)$$

5 Here, the deviatoric stress fields are calculated using ~~ESTAR~~ [the ESTAR flow relation](#) as specified in Eq. 3. When the total, rather than deformational, vorticity (i.e., without inclusion of the rigid body correction or removal of the vorticity component aligned with the flow) is used in the calculation of ~~ESTAR, the FS~~ [the ESTAR flow relation, the full-Stokes](#) analytical solution for (f_x, f_y, f_z) comprises (20 521, 9 190, 20 523) characters. By contrast, non-trivial analytical solutions for the forcing functions that are calculated from an anisotropic enhancement factor that is based on the deformational, rather than total, vorticity are at minimum 200 000 characters, well in excess of the character limits for most compilers. Accordingly, we verify ~~ESTAR~~ [our implementation of the ESTAR flow relation](#) using the total, rather than the deformational, vorticity.

To test the numerical implementation ~~of ESTAR~~, ISSM is forced using the analytical expressions for f_x , f_y , and f_z in Eqs. 18-20 and the resulting three-dimensional flow field is compared with the relevant analytical specification in Eqs. 13-17. Since the aim is to verify correct coding of the ~~ESTAR~~ [modifications within ISSM](#) ~~,~~ [for the ESTAR flow relation](#) we apply the analytic velocities on the faces as the boundary conditions. Four sets of element sizes are used for each of the ~~FS and HO~~ [full-Stokes and higher-order](#) models, increasing in resolution from 0.2 (272 elements over 5 vertical layers) to 0.08 (4656 elements over 13 vertical layers). We find convergence powers of 2.5 (v_x), 3.1 (v_y), and 2.6 (v_z) for ~~FS~~ [full-Stokes](#), respectively, and 1.4 (v_x) and 1.1 (v_y) for ~~HO~~ [higher-order](#) (Fig. 2), which are consistent with theory ([e.g., Ern and Guermond, 2004](#)) and verify our implementation.

20 6 Application of [the ESTAR flow relation](#) to idealised scenarios

~~ESTAR~~ [The ESTAR flow relation](#) was applied to a suite of test cases. The first case we present simulates flow in an embayed ice shelf; the second two are based on experiments from the Ice Sheet Model Intercomparison Project for Higher Order Models (ISMIP-HOM; Pattyn et al., 2007). The ISMIP-HOM experiments describe idealised scenarios of ice flow where the bed topography or basal friction vary. ISSM has already been validated against the ISMIP-HOM experiments (Larour et al., 2012).

25 In each experiment, the velocity, surface, and thickness fields were allowed to run to steady-state, as defined in the corresponding section below (the original ISMIP-HOM experiments were simply diagnostic). The ice sheet is isothermal in each case.

As mentioned above, we use ~~ESTAR~~ shear and compression enhancement factors of $E_S = 8$ and $E_C = 3$, respectively (Treverrow et al., 2012). For each experiment, we performed simulations using a range of Glen enhancement factors (1, 3, 30 5, and 8), but since these idealised experimental systems have simple scaling properties under global changes in flow rates,

we present only results for $E_G = 8$ since that proved the most directly relevant value. The ISMIP-HOM experiments used the original parameter values (Pattyn et al., 2007) unless otherwise indicated.

6.1 Flow through an embayed ice shelf

The first experiment simulates three-dimensional flow through a rectangular embayed ice shelf. The experiment was carried out for model domains with transverse spans $x \in [0, L]$, for $L = 20, 60,$ and 100 km and along-flow dimension $y \in [0, 100]$ km. The initial ice thickness decreases uniformly from 1000 m at the grounded zone to $300, 600,$ and 850 m at the ice front for the $L = 20, 60,$ and 100 km cases, respectively. The main features of the anisotropic effects are similar regardless of aspect ratio. This is principally because wider embayed ice shelves are flatter so that the influence of simple shear stresses on the dynamics is not particularly sensitive to aspect ratio. Accordingly, we focus our discussion on one transverse length scale: $L = 20$ km. The plan view mesh is extruded ten quadratically-spaced layers in the vertical. A no-slip boundary condition is applied along the $x = 0$ and $x = L$ side boundaries. At the inflow boundary, the y -component of velocity is set to

$$v_y(x, 0) = V_0 e^{-\left[\frac{5(x-x_{\text{mid}})}{2L}\right]^8},$$

by

$$V(x) = V_0 e^{-\left[\frac{5(x-x_{\text{mid}})}{2L}\right]^8}, \quad (21)$$

$$v_y(x, 0) = V(x) - V(0), \quad (22)$$

where $V_0 = 100 \text{ m yr}^{-1}$ and $x_{\text{mid}} = L/2$. This ensures that $v_y(x, 0)$ satisfies the no-slip boundary condition on the margins. As is standard, ocean water pressure is applied at the ice-ocean interface where tangential (traction) stresses vanish. It is assumed that there is no surface or basal melting or accumulation over the ice shelf domain. The flow parameter $A(T') = 1.74 \times 10^{-25} \text{ Pa}^{-3} \text{ s}^{-1}$, is set using the Budd and Jacka (1989) value for an isothermal ice shelf of -20 °C. We consider the case where the Glen enhancement factor is equal to the ESTAR shear enhancement factor, i.e., $E_G = E_S = 8$.

We run the HO-higher-order ice flow model for each of the ESTAR and Glen rheologies-flow relations to steady-state, which we define to be reached when the mean velocity change over the surface mesh points is less than $1 \times 10^{-2} \text{ m yr}^{-1}$ between two consecutive time steps (of $\Delta t = 2 \text{ yr}$).

The Glen and ESTAR HO-higher-order steady-state surface velocity magnitudes are compared in Fig. 3. The patterns of ice flow are similar for the two rheologies: in each case the ice velocity increases as it flows through the ice shelf, reaching its maximum at the ice front. Over most of the domain the velocities are in close agreement, reflecting the dominance of the shear flow. However, the Glen velocities are up to 17% larger than the ESTAR velocities at the ice front, where the flow field is predominantly extensive-tensile in accordance with the ice front boundary conditions. The differences in velocities can be attributed to differences in flow enhancement factors for simple shear and compression. Near the centre line of the ice shelf and across the ice front, where longitudinal and vertical normal stresses dominate, the Glen enhancement is as much as 8/3 times larger than the corresponding ESTAR enhancement.

The steady-state thickness ~~ratio for the two rheologies is shown in Fig~~ patterns for each flow relation, and their ratio are shown in Figs. 3d-d-f. In both cases, the equilibrated ice shelf is thicker along the centre line and thinner towards the side margins where ice flow is slower, and thicknesses agree within 5% over much of the domain. However, the Glen ice shelf is consistently thinner than the ESTAR ice shelf, particularly along the centre line where Glen velocity is enhanced relative to ESTAR the ESTAR case, and it is up to 20% thinner at the ice front.

The ESTAR strain rate components are presented in Fig. 4. As expected, shear strain rate in the $x - y$ plane is very high near the lateral boundaries (Fig. 4d). However, it dominates the effective strain rate (and hence λ_S) well beyond those margins (Fig. 5), before decreasing towards the centre line, where it identically vanishes. Towards the ice-ocean front, each of the normal strain rates – $\dot{\epsilon}_{xx}$, $\dot{\epsilon}_{yy}$, and $\dot{\epsilon}_{zz}$ – increase in magnitude, reaching their maxima at the front. The (approximately) longitudinal $\dot{\epsilon}_{yy}$ is the dominant normal strain rate component and is extensive-extensional towards the front. Due to the confined geometry, towards the front $\dot{\epsilon}_{yy}$ is largely balanced by $\dot{\epsilon}_{zz}$, which drives ice shelf thinning. Transverse normal strain rate $\dot{\epsilon}_{xx}$ plays a lesser role at the ice-ocean front than the other normal strain rates. It is extensive-extensional along the front as the streamlines diverge, but changes sign to compressive towards the corners. The patterns in the component strain rates, including the dominance of normal strain rates in the centre of the ice shelf and at the ice-ocean front, are evident in the strain rate on the non-rotating shear plane ($\dot{\epsilon}'$) and the effective strain rate ($\dot{\epsilon}_e$), the ratio of which sets the magnitude of λ_S (Fig. 5). In the ESTAR-embayed ice shelf simulation using the ESTAR flow relation, the vanishing of basal traction and the depth independent nature of the inflow velocity lead to an almost 2D flow field with local non-rotating shear planes essentially vertical where they can be defined – there being neither $x - y$ plane shear nor vorticity along the centre line. We note that $\dot{\epsilon}_{yy}$ decreases in magnitude with depth at the ice-ocean front, coincident with ice front tilting (Weertman, 1957), which also gives rise to some local shear deformation in the $y - z$ plane.

To assess the computational demands of the full ISSM model with ESTAR, the FS the ESTAR flow relation, the full-Stokes ice flow model was computed for one model year (i.e., steady state had not yet been reached) and the results compared with the HO higher-order simulation results for the same model period (results not shown). At the ice front, the HO higher-order velocities are everywhere within 5% of the FS full-Stokes velocities, with the maximum differences occurring near the lateral boundaries. Across the shelf, the HO higher-order component velocities accord well with the FS full-Stokes velocities. The magnitude and spatial patterns of $\dot{\epsilon}'$, $\dot{\epsilon}_e$, and λ_S also agree well between the FS and HO full-Stokes and higher-order models.

Computation times for FS full-Stokes simulations using each of the two rheologies flow relation, and for increasing mesh resolutions, are summarised in Table 1. In each case, the model was run for 1 month with a time step of $\Delta t = 1 \times 10^{-4}$ yr. The ESTAR simulation computation times are no more than 3% slower-longer than the corresponding Glen times-times for the Glen relation, and the simulation times for the two rheologies flow relations converge as the mesh resolution increases. This result gives us confidence that ESTAR the ESTAR flow relation is essentially as computationally-efficient-computationally efficient as the Glen rheology relation.

6.2 ISMIP-HOM experiment B: two-dimensional flow over a bumpy bed

ISMIP-HOM Experiment B (ISMIPB) describes two-dimensional flow (x horizontal, z vertical) over a bed topography that varies sinusoidally, according to the following equation

$$z_b(x) = z_s(x) - 1000 + 500 \sin\left(\frac{2\pi x}{L}\right). \quad (23)$$

5 where $z_s(x) = -x \tan \alpha$, for a mean bed slope of $\alpha = 0.5^\circ$, and L controls the scale of the bedrock undulation. We take $z_s(x)$ as the initial surface so that the mean initial ice thickness is 1000 m. We present results for two different aspect ratios, $L = 20$ km and $L = 5$ km, to explore the influence of different longitudinal stresses. In each case we used the full-Stokes (FS) version of ISSM. The flow parameter is fixed at $3.96 \times 10^{-25} \text{ Pa}^{-3} \text{ s}^{-1}$, corresponding to an ice temperature of approximately -14° C (Budd and Jacka, 1989). The value for the flow parameter in the original ISMIPB was $3.17 \times 10^{-24} \text{ Pa}^{-3} \text{ s}^{-1}$, which
 10 corresponds to a Budd and Jacka (1989) ice temperature of approximately -3.6° C . We have reduced the original flow parameter by a factor of 8 (i.e., equal to E_S) to ensure our results are as close as possible to the original ISMIP-HOM experiments. Periodic boundary conditions are applied at the vertical edges of the domain and a no-slip boundary condition is applied at the base. In this and the following two-dimensional test case, the normal to the non-rotating shear plane is simply the direction perpendicular to the velocity and there is no uncertainty about the vorticity (which has only one non-vanishing component)
 15 being perpendicular to the velocity. Steady-state is regarded as reached when the mean velocity change over the surface mesh points is less than $1 \times 10^{-2} \text{ m yr}^{-1}$ between two consecutive time steps of $\Delta t = 1 \text{ yr}$ for this and the following ISMIP-HOM experiment.

In what follows, we consider the case when the Glen enhancement factor is equal to the ESTAR shear enhancement factor, i.e., $E_G = E_S = 8$. This is the most relevant case for the ISMIPB experiment as the dynamics here are driven by bed-parallel
 20 shear, as discussed below.

The ESTAR and Glen FS full-Stokes steady-state horizontal velocities (v_x) for ISMIPB for $L = 20$ km are shown in Fig. 6a and b, with their ratio in Fig. 6c. The shear fraction (λ_S) used to calculate the ESTAR enhancement is shown in Fig. 6d. The ESTAR velocities are marginally slower than the Glen velocities throughout the domain, regionally by as much as 6%. While in a real-world situation, a local difference of 6% may not be significant to overall flow, clearly unless the Glen enhancement
 25 factor is approximately E_S there would be a significant and widespread difference in velocities. One major contrast occurs either side of the topographic bump in the near-surface layers (Fig. 6c) where normal stresses dominate ($\lambda_S < 1$; Fig. 6d) and $E(\lambda_S)$ tends to $E_C < E_G$, as λ_S tends to 0. This reduces the shear deformation in the upper-layers for ESTAR compared to Glen, leading to slightly lower horizontal velocities near the surface. We will discuss the relevance of this in Sect. 7. Another major velocity contrast occurs in the lowest part of the ice sheet directly above the topographic depression. Since deformation
 30 here is clearly shear dominated ($\lambda_S = 1$ for essentially the whole column), the differences must arise from a varying but consistently lower shear stress profile in the ESTAR case, reflecting indirectly the distributed effect of the stiffer ice in the upper layers where $E(\lambda_S) < E_G$ and a slightly different final geometry of the ice surface. In contrast, the closest agreement between the two velocity distributions is in the basal region over the topographic high.

Figure 6 also shows the **FS-full-Stokes** $\dot{\epsilon}_{xz}$ and $\dot{\epsilon}_{xx}$ strain rates for the **ESTAR-simulation** simulation using the ESTAR flow relation: effectively the shear and normal strain rates. The dominance of high values of λ_S indicates that bed-parallel simple shear is the main driver of ice flow in ISMIPB with the expected transition through the ice column from compression/extension-dominated flow near the surface to shear-dominated flow near the non-slip bed. Note that while the component strain rates are presented in the background cartesian frame, λ_S denotes the relative importance of simple shear on local non-rotating shear planes. Peaks in λ_S appear directly over the topographical bump and depression, extending further into the surface layers than in surrounding regions. The locations of the peaks in λ_S correspond to the transitions between **extensive-tensile** and compressive longitudinal stresses, centred on “transition curves” (Fig. 6e), along which normal strain rates are identically zero.

In addition to the case where $L = 20$ km, we also investigated the impact of reducing the horizontal extent to $L = 5$ km. In this steeper bed scenario (Fig. 7), the **ESTAR-surface-velocities** surface velocities in the ESTAR case are at least 11% slower than the Glen velocities in the surface layers across the whole domain, as much as 20% slower around the topographic bump, and up to 25% slower in the topographic depression (Fig. 7c). The much greater reductions in the magnitude of the ESTAR velocities for $L = 5$ km are a consequence of the increasing importance of longitudinal stresses in the stress balance equations for the smaller aspect ratio (Fig. 7e), and also in some areas the lower strain rates, which lead to correspondingly stiffer ice. Indeed we see a clear decline in the shear strain rate in the lower part of the bed depression in Fig. 7f, in contrast to Fig. 6f. The qualitative pattern of the longitudinal strain-rates in Fig. 7e is similar to the $L = 20$ km case, although the horizontal gradients are naturally accentuated, and the “transition curves” are displaced.

In order to examine the dynamics giving rise to the high shear-dominance peaks in Fig. 6d and Fig. 7d, we consider the following exact form of λ_S^2 (for these two-dimensional flow fields) expressible using the cartesian frame strain rate components

$$\lambda_S^2 = \frac{\alpha \dot{\epsilon}_{xx}^2 + \beta \dot{\epsilon}_{xz}^2 + \gamma \dot{\epsilon}_{xx} \dot{\epsilon}_{xz}}{\dot{\epsilon}_{xx}^2 + \dot{\epsilon}_{xz}^2}, \quad (24)$$

for some spatially varying coefficients α , β , and γ . Since there is no surface accumulation, velocities and hence local non-rotating shear planes at the ice sheet surface are parallel to the surface. The traction free surface boundary condition implies that the numerator ($\dot{\epsilon}'^2$) in Eq. 24, and accordingly λ_S , vanishes at the surface, except that if $\dot{\epsilon}_e$ also vanishes, λ_S is technically undefined. Our implementation sets $\lambda_S = 0$ for vanishing $\dot{\epsilon}'$ in such situations. It is apparent from Eq. 24 that along the transition curves, i.e., where $\dot{\epsilon}_{xx} = \dot{\epsilon}_{zz} = 0$, $\lambda_S^2 = \beta$, independent of (non-zero) $\dot{\epsilon}_{xz}$ strain rate. One can show that $\beta \rightarrow (1 - S_x^2)^2$ towards the surface (i.e., for surface slope in the x -direction S_x) along the transition curve, in order to satisfy the surface boundary condition. This indicates that λ_S would be finite along the transition curves all the way to the surface, except that we enforced its vanishing there. For these locations, the Glen and ESTAR viscosities corresponding to Eqs. 2-3 would tend to infinity as $\dot{\epsilon}_e$ vanished approaching the surface, but are limited to a maximum value in the ISSM implementation.

Note that away from the transition curves λ_S goes to zero as we approach the surface, associated with vanishing shear on the non-rotating shear plane and the corresponding dominance of normal deformations. We return to these near-surface spikes in λ_S in the discussion.

6.3 ISMIP-HOM experiment D: two-dimensional flow over a sticky spot

ISMIP-HOM experiment D (ISMIPD) describes a two-dimensional domain over which the basal friction coefficient χ varies sinusoidally in the horizontal direction. A Paterson-type friction law ([Paterson, 1994](#)) ([Paterson, 1994, p.151](#)) of the following form is used

$$5 \quad \tau_b = -\chi^2 v_b, \quad (25)$$

where τ_b is the basal stress and v_b the basal velocity, and the friction coefficient, χ^2 (Pa a m^{-1}), varies according to the equation

$$\chi^2 = 1000 + 1000 \sin\left(\frac{2\pi}{L}x\right). \quad (26)$$

The bed topography and the initial ice surface are inclined planes with a slope of 0.1° , and the initial thickness is 1000 m throughout the domain. As in the preceding ISMIPB experiments, the flow parameter is taken as $A(T') = 3.96 \times 10^{-25} \text{ Pa}^{-3} \text{ s}^{-1}$ (the ISMIPB and ISMIPD original flow parameters were equal). Periodic boundary conditions are applied at the edges of the domain. Once again, we present results for steady-state solutions for two different horizontal scales: $L = 20 \text{ km}$ and $L = 5 \text{ km}$. As with the ISMIPB experiments above, we employ the full-Stokes (**FS**) solver in ISSM. Consistent with ISMIPB, the control of the final deformation flow in the ISMIPD experiment is bed-parallel shear, so we consider the case when the Glen enhancement factor is equal to the ESTAR shear enhancement factor, i.e., $E_G = E_S = 8$.

The Glen and ESTAR **FS-full-Stokes** results for ISMIPD when $L = 20 \text{ km}$ are shown in Fig. 8. **For both rheologies** In both cases, the fastest velocities develop in the upper part of the column over the sticky spot (centred around 5 km). This is required by continuity, given the lower basal velocities over the sticky spot, to balance the block flow over the slippery section (basal friction coefficient vanishes at 15 km). The basal velocities increase as the basal friction coefficient decreases. The total steady-state ESTAR velocities are everywhere within 1% of the corresponding Glen velocities (see Fig. 8c), with the maximum difference occurring in the near-surface layers over the sticky spot, where the **ESTAR** ice is stiffer in the ESTAR case, as shown by the corresponding contrast in viscosities (Fig. 8e). Sliding occurs throughout the domain and the deviations from block flow are modest throughout, so to explore what differences might be associated with the departure from block flow we calculated “deformational velocities” from v_x by subtracting the basal motion, and examined the ratio between ESTAR and Glen cases (Fig. 8d). The most notable feature of this ratio is a localised 50% decrease in deformational velocity for ESTAR compared to Glen through the entire column, peaking directly over the point where the basal friction coefficient (Eq. 26) vanishes. This major band of difference coincides with the band of higher viscosity for ESTAR, relative to Glen, (see Fig. 8e) over the slippery region.

The ESTAR component strain rates and shear fraction λ_S are illustrated in Fig. 9 for ISMIPD, for the $L = 20 \text{ km}$ case. The plot of λ_S (Fig. 9d) depicts transitions in the deformation regime from shear-dominated to compression/extension-dominated and back over a few kilometres around the slippery spot. These transitions extend all the way to the bed, becoming perpendicular to the ice flow direction and reflect the low shear over the slippery region. This is in marked contrast to the ISMIPB experiments, where the shear deformation regime dominated except near the free surface. We in the next section we discuss the

implications of these abrupt transitions for the assumptions that underpin ~~ESTAR in the next section~~ [the ESTAR flow relation](#). Shear dominates much of the ice column ($\lambda_S > 0.5$) throughout the rest of the domain (over the region where values of the basal friction coefficient exceed 10% of the maximum value). The shear strain rates are greatest in the region of maximum stickiness at approximately 5 km, and a steep profile in the shear strain rate is present there. Naturally, transitions between [extensive-tensile](#) and compressive flows occur around the sticky spot and the transition curves (vanishing normal strain rates) resemble the ISMIPB cases (Fig. 6e). Here the transition curves reach the surface as the friction coefficient increases, and just downstream of its peak value (the sticky spot), leading to ~~near-surface~~ [near-surface](#) spikes of high values λ_S analogous to ISMIPB. It should be noted that the strain rates here are very small compared to the ISMIPB experiments. The viscosity ratio in Fig. 8e reveals that there are also lower strain rates for ~~ESTAR~~ [the ESTAR case](#) in the compression dominated regions, as the ratios there are higher than the factor of 1.39 that would be produced by the influence of $E(\lambda_S)$ alone.

The results of a [FS-full-Stokes](#) prognostic run to steady-state for the ISMIPD experiment for $L = 5$ km are presented in Fig. 10. The v_x velocity ratio (Fig. 10c) shows that very little difference is seen between results for the two flow relations, unlike the ISMIPB experiments in the previous section, where differences up to 25% between ESTAR and Glen cases emerged for the shorter bedrock periodicity. The tiny differences in overall velocities are enhanced but the patterns in Fig. 8c and Fig. 10c are similar. However, there is a significantly different picture in the ratio of deformation velocities seen in Fig. 10d, compared to Fig. 8e. The largest differences are now limited to the lower portion of the ice column and for much of the region over the slippery bed the ratio is almost unity.

The pattern of deformation regimes mapped by λ_S (Fig. 10f) is also more complex than that seen in the preceding $L = 20$ km case (see Fig. 9d). The general structure of the normal strain rates is similar to previous experiments, but here the persistence of a band of shear (Fig. 10h) above the slippery spot at intermediate depths prevents the establishment of a vertical block of flow dominated by normal stresses. The shear profile above the sticky spot is also much weaker in the upper layers. Accordingly, λ_S reveals a band of unevenly shear-dominated deformation which is continuous across the periodic domain. Once again, shear dominated spikes extend towards the surface in association with the vanishing of the normal strain rates.

The spatial variations in the viscosity ratio (Fig. 10e) depart significantly from those of λ_S , reflecting more strikingly than for $L = 20$ km (Fig. 8e) the combined influence of the pattern of enhancement (controlled by $E(\lambda_S)$) and the effect of different strain rates, with values both above and below the range (1.0-1.39) directly controlled by $E(\lambda_S)/E_G$.

7 Discussion

In this study we conducted various ice flow simulations, comparing ~~ESTAR with the isotropic Glen flow relation~~ [ESTAR the ESTAR and Glen flow relations](#). [The ESTAR flow relation](#) incorporates the observed differences between tertiary deformation rates for shear dominated and normal stress dominated stress regimes.

Our simulations of embayed ice shelf flow showed that no single Glen enhancement factor (E_G) can reproduce the anisotropic flow characteristic of the various stress regimes encountered. Significantly, while a choice of $E_G = E_S$ was necessary to reproduce the same overall velocities and ice thicknesses, which are largely controlled by lateral shear, this overestimated velocities

near the ice front by up to 17% compared to ~~ESTAR~~the results using the ESTAR flow relation. This is a consequence of softer ice in the Glen case for the zone near the ice front, where extensional longitudinal stresses dominate. The steady-state Glen ice shelf was accordingly up to 20% thinner than the ESTAR ice shelf in this region. Even with this thinner ice influencing the ocean pressure boundary condition at the ice front, the softer ice in the Glen case meant that the longitudinal strain rates there
5 were higher.

These results highlight one of the key failures of the Glen flow relation: an inability to account for complex, spatially varying stress regimes in its prescription of ice flow. The addition of an enhancement factor E_G to the Glen flow relation permits some compensation for the flow enhancement associated with microstructural development (i.e., rescaling the minimum creep rate data conventionally used in prescribing the Glen flow relation, e.g., Table 3.3, ~~Cuffey and Paterson,~~
10 ~~2010~~Cuffey and Paterson, 2010). However, such a modification does nothing to allow for the ~~anisotropic~~ (stress configuration dependent) ~~)-~~aspects of ice ~~rheology~~deformation rates, associated with the development of anisotropic crystal fabrics, that are characteristic of tertiary creep. The improvement offered by ~~ESTAR~~the ESTAR flow relation is that the specification of the pattern and degree of enhancement is physically based, varying spatially as a function of the stress configuration. This is achieved without the complication of a detailed treatment of microstructural information.

15 The ISMIP-HOM experiments B and D simulated scenarios in which the dominant control of flow was bed-parallel simple shear. In the prognostic runs with the larger aspect ratio ($L = 20$ km), only small differences were apparent between the Glen and ESTAR velocities ($< 6\%$ for ISMIPB and $< 1\%$ for ISMIPD), again provided the Glen enhancement factor was chosen equal to the ESTAR shear enhancement factor ($E_G = E_S$).

For more rapidly varying bed topography in ISMIPB, with $L = 5$ km, the differences in velocity for the two flow relations
20 reached 25%, with surface variations of 11%. For ISMIPD, which explored variations in basal friction, the $L = 5$ km experiments still showed $< 1\%$ differences in velocities with very low strain rates, so that although a complex pattern of deformation regimes emerged, there was little effect on flow from the choice of flow relation.

These results suggest if major bed topography ~~only varied~~varied only on scales much longer than the ice thickness, close agreement between ~~ESTAR and the Glen flow relation~~simulations using ESTAR and Glen flow relations might be achieved
25 more generally by choosing the tertiary shear enhancement factor as the Glen enhancement factor ($E_G = E_S$). This might provide a physical rationale to replace the *ad hoc* enhancement factors typically used in large-scale grounded ice sheet modelling with the value appropriate to flow dominated by simple shear. However, larger differences between velocities and vertical shear profiles emerged for the more rapid bedrock variation, where the importance of including longitudinal stresses in the momentum balance is already recognised (Pattyn et al., 2008), suggesting that adopting ~~ESTAR~~the ESTAR flow relation would be
30 preferable.

Our idealised test cases also provide some insights into the validity of the tertiary flow assumption underlying ~~ESTAR~~the ESTAR flow relation, and the development of anisotropic crystal fabrics compatible with the current deformation regime. In the embayed ice shelf test the most significant change in the deformation regime is clearly the transition to ~~extensive~~extensional
35 ice experiences gradual changes in stress regime, and the magnitudes of strain rates (e.g., Fig. 4b) and velocities (Fig. 3)

indicate that in the region near the ice front, where the results for the Glen and ESTAR results vary flow relations differ appreciably, a progression of essentially compatible fabrics would be maintained. Indeed, under the prevailing deformation and flow conditions these would even develop from random fabrics over a few km.

5 The ISMIP-HOM experiments reveal potential violations of the tertiary flow assumption, although the significance for the flow field of these apparent short-comings needs to be assessed with regard to the somewhat artificial nature of the tests. Indeed as we saw, the difference between the ESTAR predictions and the results of the ESTAR and Glen flow relations (provided $E_G = E_S$) was small, except for ISMIPB with $L = 5$ km, although of course ESTAR the ESTAR flow relation makes no claim to correctly describe the transient rheology deformation rates of ice with an evolving anisotropy.

10 The ISMIP experiments have a spatial periodicity, which could allow one portion of the repetitive basal conditions to dominate the overall flow. Also, there is no surface mass budget in these experiments so that, as remarked earlier, the ice surface is a flow-line streamline, whereas in a system with surface accumulation fresh snow is always being added and advected down into the ice sheet where it makes the transition to solid ice. Accordingly, in the flow regime of these prognostic experiments even the surface layers would be regarded as having developed some anisotropy just as the lower layers would, since they have in principle been deforming over an arbitrarily long time.

15 The main issue about the establishment of tertiary flow conditions in the periodic environment of our ISMIP experiments concerns the possible cycling of the flowing ice through a variety of stress regimes. This leads to transition regions where the stress regime and presumably the crystal anisotropy would be evolving, and the compatibility assumptions behind ESTAR could the ESTAR flow relation would locally be violated. Clearly the spatial extent of transitional flow and the delay in attaining any new tertiary state depends on the magnitudes of the strain rates and the velocity of the ice. By combining these with a threshold
20 for accumulated strain as the criterion for development of a compatible (tertiary) fabric under a persistent flow regime, the extent of a transition zone can be estimated. This scale can then be compared to the horizontal variation of the stress regime. Selecting the 10% strain required to develop a compatible anisotropy from initially randomly oriented ice should provide a conservative yardstick, when applied to gradual changes in stress regime.

25 The patterns of stress regimes revealed by the distributions of λ_S (Figs. 6d, 7d, 9a, and 10f) indicate where along-flow variations in stress regime might be too rapid to sustain the assumption that a compatible crystallographic anisotropy had evolved. For the ISMIPB experiments this concern is essentially focussed to the near surface spikes in λ_S around the two locations where longitudinal deformations vanish, since the anisotropy of deeper ice will be compatible with deformation dominated by simple shear. There may be some complications with a slow cycling of the upper levels between extensive tensile and compressive flow. Very near the surface, the λ_S peak intervals are narrow and the shear strain rates there are very
30 small (corresponding to transition scales of several kilometres) so that there will be no appreciable development of a shear compatible fabric. Either side of the peaks, the main extensive-tensile and compressive flow domains for $L = 20$ km (see Fig. 6e) are ≈ 5 km long and have transition scales of < 1 km which suggests that the strongly normal stress dominated upper layer will be mainly in tertiary state. Turning to the transient shear intrusions into this layer: at 100 m depth over the bump the shear transition scale is ≈ 3 km while at 200 m depth over the depression the shear transition scale is ≈ 5 km, suggesting that
35 that the λ_S peaks do represent a local failure of ESTAR the ESTAR flow relation's tertiary assumption. Throughout the domain

the lower half of the ice column has transition scales of ≤ 300 m which, given the gradual variations in λ_S and the direction of ice flow, indicates that region is in the tertiary state.

For ISMIPB with $L = 5$ km, which displays a generally deeper band of normal stress dominated regime (Fig. 7d), the transition scales for the compressive and ~~extensive-tensile~~ regions are ~ 500 m for regions of ≈ 1 km in extent, while the shear transition scales at 100 m depth above the bump and 200 m depth above the depression are now ~ 10 km and ~ 1 km, respectively. For most of the domain the transition rates in the lower half of the ice column are ≤ 100 m, although this rises to nearly 1000 m above the bedrock bump.

In the ISMIPD case, for $L = 20$ km, the pattern of λ_S (Fig. 9a) shows there are also transitions between simple shear dominated and extension dominated deformation associated with the slippery region, with varying abruptness at different depths, and some of the contours of λ_S in this instance almost orthogonal to the ice flow. A complication is that there is very little longitudinal deformation (Fig. 9e) occurring over the slippery region because the overall flow is controlled by the periodic sticky spot. Accordingly, there would not be any significant fabric evolution across this ~ 4 km region (estimated transition scales there are > 40 km) so that the tertiary assumption and using E_C (since $\lambda_S = 1$) would be inappropriate. Once again, the low strain rates here (Figs. 9e-f) translate into very stiff ice and might make the influence of ESTAR enhancement factors relatively unimportant. A factor of 100 in $\dot{\epsilon}_e$ changes viscosity by a factor of 21.5, whereas the maximum viscosity contrast from $E(\lambda_S)$ is 1.39. The shear strain rates are also very low, with transition scales > 1 km except very close to the bed over the sticky spot. Accordingly, while a compatible fabric could be expected where the large λ_S values are shown in Fig. 6a, its presence would be due to the periodic flow, and the inability of the $\lambda_S \sim 0$ region to modify it.

For the last test, ISMIPD with $L = 5$ km, strain-rates are once again very low, and there is no simple structure to the picture of the stress regime portrayed by λ_S in Fig. 10f. Below mid-depth there is a periodically continuous band of shear that might favour the development of crystal anisotropy, but clearly the tertiary flow assumption of ~~ESTAR-the ESTAR flow relation~~ would not be particularly useful here.

The focus of this study was to explore the effect on the dynamic response of ice sheets of using ~~an anisotropic (ESTAR) description of rheology; a constitutive relation appropriate to the tertiary flow regime, i.e.~~ sensitive to the varying proportions of simple shear and normal stresses, compared to using the standard (Glen) ~~isotropic description of rheology flow relation~~. Our results, particularly with respect to the differences between the Glen and ESTAR simulations, are sensitive to the choice of E_S and E_C . Experimental evidence (Treverrow et al., 2012) suggests that the ratio $E_S/E_C = 8/3$, rather than their overall magnitude, is the dominant control in the level of enhancement $E(\lambda_S)$ and corresponding dynamic response of grounded and floating ice sheets. Here, we used values of $E_S = 8$ and $E_C = 3$, which are based on laboratory experiments of tertiary creep (Treverrow et al., 2012), and which yield values for the overall enhancement that are compatible with estimates from borehole inclination measurements (e.g., Russell-Head and Budd, 1979) and modelling studies (e.g., Wang and Warner, 1999). Nevertheless, further investigation into suitable values of E_S and E_C to use in numerical modelling studies of grounded and floating ice sheets is warranted. Indeed, with the implementation of ~~ESTAR-the ESTAR flow relation~~ in ISSM, it might be possible to use inverse methods to ~~infer-search for~~ values of E_S and E_C that improved the match between modelled and observed surface velocities.

In order to examine the impact of ~~an anisotropic rheology~~ a flow relation appropriate to ice with a compatible flow-induced anisotropic crystal fabric on simulated ice dynamics, the ISMIP-HOM and embayed ice shelf experiments were carried out assuming isothermal conditions. However, as discussed earlier, real ice sheets and ice shelves typically have cold, upper layers and strong vertical gradients in temperature, and these will often be stronger controls on vertical contrasts in deformation rates, through $A(T')$ (Eqs. 2-3), than a factor of 3 to 8 produced by ~~anisotropic enhancement~~ enhancements for tertiary flow.

8 Conclusions

We have investigated some consequences of incorporating the flow properties of anisotropic ice into modelling flow in ice sheets and ice shelves. Specifically, we have investigated the flow response to prolonged deformation under a constant or slowly changing stress regime and the associated development of an anisotropic crystal orientation fabric compatible with that deformation, as represented by the empirical, scalar, tertiary ~~anisotropic rheology~~ constitutive relation for ice with a compatible anisotropic crystal fabric of Budd et al. (2013) – ~~ESTAR~~ the ESTAR flow relation. Having implemented this ~~rheology~~ flow relation in ISSM, we made initial studies in the context of idealised experiments: for an embayed ice shelf, and in two-dimensional models of grounded ice flow over varying topography and variable basal friction previously explored by ice flow modellers (Pattyn et al., 2007, 2008). We have demonstrated that ~~ESTAR is a computationally efficient anisotropic rheology~~ the ESTAR flow relation is computationally efficient for large-scale ice sheet models. We have highlighted that ~~ESTAR~~ it produces different flow responses compared with the prevailing ~~rheological description based on the~~ Glen flow relation, in regions where simple shear and normal stresses, and combinations of these, are drivers of ice flow. We have also noted some possible limitations of this empirical treatment of the tertiary flow regime, although their significance and whether there is scope for developing the empirical approach to resolve them remain to be determined. It would also be interesting to compare ~~ESTAR~~ the ESTAR flow relation with the predictions of modelling ~~that uses more complex rheological descriptions using~~ microstructure-controlled constitutive relations, even if the ~~comparison was~~ comparisons were limited to local domains or idealised cases.

Our embayed ice shelf results have significant implications for ice sheet model simulations that rely on the Glen flow relation to simulate past, present, and future ice flow, which are used to constrain uncertainty in reconstructions and projections of sea levels. In particular, the effect of unrealistically fast thinning ice near the calving front, as simulated with the Glen flow relation, is to deform the ice shelf, which could lead to unrealistic ice shelf geometries and affect buttressing if it were to spread beyond the “passive ice” sector (Furst et al., 2016) near the ice front.

With the implementation of ~~ESTAR~~ the ESTAR flow relation into ISSM completed, further investigation into ~~the capabilities of ESTAR~~ its capacity to replicate real-world ice sheet flow in Antarctic outlet glaciers is currently underway.

Code availability. The results from this work are reproducible using ISSM (from version 4.11). The current version of ISSM is available for download at <https://issm.jpl.nasa.gov>. The ISMIP-HOM experiments are documented in Pattyn et al. (2007).

Competing interests. The authors have no competing interests.

Acknowledgements. The authors thank ~~two anonymous~~ each of the three reviewers for their comments that resulted in an improved manuscript. This work was supported under the Australian Research Council's Special Research Initiative for Antarctic Gateway Partnership (Project ID SR140300001), and the Australian Government's Cooperative Research Centres Programme through the Antarctic Climate and Ecosystems
5 Cooperative Research Centre (ACE CRC). The University of Tasmania supported the visit of MM to Hobart. This research was undertaken with the assistance of resources from the National Computational Infrastructure (NCI), which is supported by the Australian Government.

References

- Azuma, N. and Goto-Azuma, K.: An anisotropic flow law for ice sheet ice and its implications, *Ann. Glaciol.*, 23, 202–208, 1996.
- Baker, R.: Is the creep of ice really independent of the third deviatoric stress invariant?, in: *The Physical Basis of Ice Sheet Modelling*, pp. 7–16, IAHS Publ. 170, 1987.
- 5 Blatter, H.: Velocity And Stress-Fields In Grounded Glaciers: A Simple Algorithm For Including Deviatoric Stress Gradients, *J. Glaciol.*, 41, 333–344, 1995.
- Bouchez, J. and Duval, P.: The fabric of polycrystalline ice deformed in simple shear: Experiments in torsion, natural deformation and geometrical interpretation, *Texture Microstruct.*, 5, 171–190, 1982.
- Breuer, B., Lange, M. A., and Blindow, N.: Sensitivity studies on model modifications to assess the dynamics of a temperature ice cap, such
10 as that on King George Island, Antarctica, *J. Glaciol.*, 52, 235–247, 2006.
- Budd, W. and Jacka, T.: A review of ice rheology for ice sheet modelling, *Cold Reg. Sci. Technol.*, 16, 107–144, 1989.
- Budd, W. F.: The development of crystal orientation fabrics in moving ice, *Z. Gletscherkd. Glazialgeol.*, 8, 65–105, 1972.
- Budd, W. F., Warner, R. C., Jacka, T. H., Li, J., and Treverrow, A.: Ice flow relations for stress and strain-rate components from combined shear and compression laboratory experiments, *J. Glaciol.*, 59, 374–392, doi:10.3189/2013JoG12J106, 2013.
- 15 Cuffey, K. and Paterson, W. S. B.: *The Physics of Glaciers*, 4th Edition, Elsevier, Oxford, 2010.
- DiPrinzio, C., Wilen, L., Alley, R., Fitzpatrick, J., Spencer, M., and Gow, A.: Fabric and texture at Siple Dome, Antarctica, *J. Glaciol.*, 51, 281–290, 2005.
- Donoghue, S. and Jacka, T.: The stress pattern within the Law Dome Summit to Cape Folger ice flow line, inferred from measurements of crystal fabric, in: *Physics of Ice Core Records II*, edited by Hondoh, T., pp. 125–135, Hokkaido University Press, Sapporo, 2009.
- 20 Durand, G., Gagliardini, O., Zwinger, T., Le Meur, E., and Hindmarsh, R.: Full Stokes modeling of marine ice sheets: influence of the grid size, *Ann. Glaciol.*, 50, 109–114, 2009.
- Duval, P.: Creep and fabrics of polycrystalline ice under shear and compression, *J. Glaciol.*, 27, 129–140, 1981.
- Ern, A. and Guermond, J.-L.: *Applied Mathematical Sciences*, vol. 159, chap. Theory and practice of finite elements, pp. 175–217, Springer, 2004.
- 25 Faria, S. H.: The symmetry group of the CAFFE model, *J. Glaciol.*, 54, 643–645, doi:10.3189/002214308786570935, 2008.
- Faria, S. H., Weikusat, I., and Azuma, N.: The microstructure of polar ice. Part II: State of the art, *J. Struct. Geol.*, 61, 21 – 49, doi:10.1016/j.jsg.2013.11.003, 2014.
- Furst, J. J., Durand, G., Gillet-Chaulet, F., Tavard, L., Rankl, M., Braun, M., and Gagliardini, O.: The safety band of Antarctic ice shelves, *Nat. Clim. Change*, 6, 479–482, doi:10.1038/NCLIMATE2912, 2016.
- 30 Gagliardini, O., Gillet-Chaulet, F., and Montagnat, M.: A review of anisotropic polar ice models: from crystal to ice-sheet flow models, in: *Physics of Ice Core Records II*, edited by Hondoh, T., pp. 149–166, Institute of Low Temperature Science, Hokkaido University, Sapporo, Japan, 2009.
- Gao, X. and Jacka, T.: The approach to similar tertiary creep rates for Antarctic core ice and laboratory prepared ice, *Journal de Physique, Colloque C1*, supplement to no. 3, Tome 48, pp. 289–296, 1987.
- 35 Gillet-Chaulet, F., Gagliardini, O., Meyssonier, J., Montagnat, M., and Castelnau, O.: A user-friendly anisotropic flow law for ice-sheet modelling, *J. Glaciol.*, 51, 3–14, doi:10.3189/172756505781829584, 2005.
- Glen, J.: The creep of polycrystalline ice, *Proc. R. Soc. A*, 228, 519–538, 1955.

- Glen, J.: The flow law of ice: A discussion of the assumptions made in glacier theory, their experimental foundations and consequences, IASH Publ, 47, 171–183, 1958.
- Glen, J. W.: Experiments on the deformation of ice, *J. Glaciol.*, 2, 111–114, 1952.
- Glen, J. W.: Rate of flow of polycrystalline ice, *Nature*, 172, 721–722, 1953.
- 5 Gödert, G.: A mesoscopic approach for modelling texture evolution of polar ice including recrystallisation phenomena, *Ann. Glaciol.*, 37, 23–28, doi:10.3189/172756403781815375, 2003.
- Greve, R.: Relation of measured basal temperatures and the spatial distribution of the geothermal heat flux for the Greenland ice sheet, *Ann. Glaciol.*, 42, 424–432, 2005.
- Greve, R. and Blatter, H.: *Dynamics of Ice Sheets and Glaciers*, Advances in Geophysical and Environmental Mechanics and Mathematics, Springer-Verlag, 2009.
- 10 Greve, R. and Blatter, H.: Comparison of thermodynamics solvers in the polythermal ice sheet model SICOPOLIS, *Polar Science*, 10, 11 – 23, doi:http://dx.doi.org/10.1016/j.polar.2015.12.004, 2016.
- Hudleston, P.: Structures and fabrics in glacial ice: A review, *Journal of Structural Geology*, 81, 1 – 27, doi:http://dx.doi.org/10.1016/j.jsg.2015.09.003, http://www.sciencedirect.com/science/article/pii/S0191814115300365, 2015.
- 15 Hulbe, C. L., Wang, W., Joughin, I. R., and Siegert, M. J.: The role of lateral and vertical shear in tributary flow toward a West Antarctic ice stream, *Ann. Glaciol.*, 36, 244–250, 2003.
- Huybrechts, P., Rybak, O., Pattyn, F., Ruth, U., and Steinhage, D.: Ice thinning, upstream advection, and non-climatic biases for the upper 89% of the EDML ice core from a nested model of the Antarctic ice sheet, *Clim. Past*, 3, 577–589, 2007.
- Jacka, T. and Maccagnan, M.: Ice crystallographic and strain rate changes with strain in compression and extension, *Cold Reg. Sci. Technol.*, 20 8, 269–286, 1984.
- Jaeger, J. C.: *Elasticity, fracture and flow: with engineering and geological applications*, Methuen, 3rd edn., 1969.
- Kamb, B.: *Experimental recrystallization of ice under stress*, American Geophysical Union, 1973.
- Kipfstuhl, S., Faria, S., Azuma, N., Freitag, J., Hamann, I., Kaufmann, P., Miller, H., Weiler, K., and Wilhelms, F.: Evidence of dynamic recrystallization in polar firn, *J. Geophys. Res.*, 114, B05 204, 2009.
- 25 Kocks, U. F., Tomé, C. N., and Wenk, H.-R.: *Texture and anisotropy: preferred orientations in polycrystals and their effect on materials properties*, Cambridge U. Press, 1998.
- Larour, E., Seroussi, H., Morlighem, M., and Rignot, E.: Continental scale, high order, high spatial resolution, ice sheet modeling using the Ice Sheet System Model (ISSM), *J. Geophys. Res.*, 117, 1–20, doi:10.1029/2011JF002140, 2012.
- Li, J. and Jacka, T.: Correspondence. Horizontal shear rate of ice initially exhibiting vertical compression fabrics, *J. Glaciol.*, 44, 670–672, 30 1998.
- Li, J., Jacka, J., and Budd, W. F.: Deformation rates in combined compression and shear for ice which is initially isotropic and after the development of strong anisotropy, *Ann. Glaciol.*, 23, 247–252, 1996.
- Lile, R.: The effect of anisotropy on the creep of polycrystalline ice, *J. Glaciol.*, 21, 475–483, 1978.
- Lliboutry, L.: Anisotropic, transversely isotropic nonlinear viscosity of rock ice and rheological parameters inferred from homogenization, 35 *Int. J. Plasticity*, 9, 619–632, 1993.
- Ma, Y., Gagliardini, O., Ritz, C., Gillet-Chaulet, F., Durand, G., and Montagnat, M.: Enhancement factors for grounded ice and ice shelves inferred from an anisotropic ice-flow model, *J. Glaciol.*, 56, 805–812, 2010.

- MacAyeal, D.: Large-scale ice flow over a viscous basal sediment: Theory and application to Ice Stream B, Antarctica, *J. Geophys. Res.*, 94, 4071–4087, 1989.
- Marshall, S. J.: Recent advances in understanding ice sheet dynamics, *Earth Planet. Sci. Lett.*, 240, 191–204, 2005.
- Martín, C. and Gudmundsson, G. H.: Effects of nonlinear rheology, temperature and anisotropy on the relationship between age and depth at ice divides, *The Cryosphere*, 6, 1221–1229, doi:10.5194/tc-6-1221-2012, 2012.
- 5 Montagnat, M., Azuma, N., Dahl-Jensen, D., Eichler, J., Fujita, S., Gillet-Chaulet, F., Kipfstuhl, S., Samyn, D., Svensson, A., and Weikusat, I.: Fabric along the NEEM ice core, Greenland, and its comparison with GRIP and NGRIP ice cores, *The Cryosphere*, 8, 1129–1138, doi:10.5194/tc-8-1129-2014, 2014.
- Morgan, V., Wookey, C., Li, J., van Ommen, T., Skinner, W., and Fitzpatrick, M.: Site information and initial results from deep ice drilling on Law Dome, Antarctica, *J. Glaciol.*, 43, 3–10, 1997.
- 10 Morgan, V., van Ommen, T., Elcheikh, A., and Li, J.: Variations in shear deformation rate with depth at Dome Summit South, Law Dome, East Antarctica, *Ann. Glaciol.*, pp. 135–139, 1998.
- Morland, L.: The general viscous relation for the response of ice and its implications in the reduced model for ice-sheet flow, *Journal of Glaciology*, 53, 435–441, doi:10.3189/002214307783258413, 2007.
- 15 Nye, J. F.: The flow law of ice from measurements in glacier tunnels, laboratory experiments and the Jungfraufirn borehole experiment, *Proc. R. Soc. A*, 219, 477–489, 1953.
- Paterson, W.: *The Physics of Glaciers*, Pergamon Press, Oxford, London, New York, 3rd edn., 1994.
- Pattyn, F.: A new three-dimensional higher-order thermomechanical ice sheet model: Basic sensitivity, ice stream development, and ice flow across subglacial lakes, *J. Geophys. Res.*, 108, 1–15, doi:10.1029/2002JB002329, 2003.
- 20 Pattyn, F., Perichon, L., Aschwanden, A., Breuer, B., De Smedt, B., Gagliardini, O., Hindmarsh, R., Hubbard, A., Johnson, J., Kleiner, T., Konovalov, Y., Martin, C., Payne, T., Pollard, D., Price, S., Saito, F., and Sugiyama, S.: ISMIP-HOM: Results of the Higher-Order Ice Sheet Model Intercomparison Project, in: *European Geosciences Union*, 2007.
- Pattyn, F., Perichon, L., Aschwanden, A., Breuer, B., de Smedt, B., Gagliardini, O., Gudmundsson, G. H., Hindmarsh, R. C. A., Hubbard, A., Johnson, J. V., Kleiner, T., Konovalov, Y., Martin, C., Payne, A. J., Pollard, D., Price, S., Rückamp, M., Saito, F., Soucek, O., Sugiyama, S., and Zwinger, T.: Benchmark experiments for higher-order and full-Stokes ice sheet models (ISMIP-HOM), *The Cryosphere*, 2, 95–108, 2008.
- 25 Pettit, E., Thorsteinsson, T., Jacobson, H., and Waddington, E.: The role of crystal fabric in flow near an ice divide, *J. Glaciol.*, 53, 277–288, doi:10.3189/172756507782202766, 2007.
- Pimienta, P., Duval, P., and Lipenkov, V. Y.: Mechanical behaviour of anisotropic polar ice, in: *The Physical Basis of Ice Sheet Modelling*, pp. 57–65, IAHS Publ. 170, 1987.
- 30 Placidi, L., Greve, R., Seddik, H., and Faria, S.: Continuum-mechanical, Anisotropic Flow model, for polar ice masses, based on an anisotropic Flow Enhancement factor, *Continuum Mech. Thermodyn.*, 22, 221–237, doi:10.1007/s00161-009-0126-0, 2010.
- Russell-Head, D. and Budd, W.: Ice-sheet flow properties derived from bore-hole shear measurements combined with ice-core studies, *J. Glaciol.*, 24, 117–130, 1979.
- 35 Saito, F. and Abe-Ouchi, A.: Thermal structure of Dome Fuji and east Dronning Maud Land, Antarctica, simulated by a three-dimensional ice-sheet model, *Ann. Glaciol.*, 39, 433–438, 2004.
- Schmid, E. and Boas, W.: *Plasticity of crystals*, F.A. Hughes and Co. Ltd., London, 1950.

- Seddik, H., Greve, R., Zwinger, T., and Placidi, L.: A full Stokes ice flow model for the vicinity of Dome Fuji, Antarctica, with induced anisotropy and fabric evolution, *The Cryosphere*, 5, 495–508, doi:10.5194/tc-5-495-2011, 2011.
- Staroszczyk, R. and Gagliardini, O.: Two orthotropic models for strain-induced anisotropy of polar ice, *J. Glaciol.*, 45, 485–494, 1999.
- Thorsteinsson, T.: An analytical approach to deformation of anisotropic ice-crystal aggregates, *J. Glaciol.*, 47, 507–516, 2001.
- 5 Thorsteinsson, T.: Fabric development with nearest-neighbour interaction and dynamic recrystallization, *J. Geophys. Res. - Solid Earth*, 107, doi:10.1029/2001JB000244, 2002.
- Thorsteinsson, T., Waddington, E. D., and Fletcher, R. C.: Spatial and temporal scales of anisotropic effects in ice-sheet flow, *Ann. Glaciol.*, 37, 40–48, 2003.
- Treverrow, A., Budd, W. F., Jacka, T. H., and Warner, R. C.: The tertiary creep of polycrystalline ice: experimental evidence for stress-dependent levels of strain-rate enhancement, *J. Glaciol.*, 58, 301–314, doi:10.3189/2012JoG11J149, 2012.
- 10 Treverrow, A., Warner, R. C., Budd, W. F., Jacka, T. H., and Roberts, J. L.: Modelled stress distributions at the Dome Summit South borehole, Law Dome, East Antarctica: a comparison of anisotropic ice flow relations, *J. Glaciol.*, 61, 987–1004, doi:10.3189/2016JoG14J198, 2015.
- Treverrow, A., Jun, L., and Jacka, T. H.: Ice crystal c-axis orientation and mean grain size measurements from the Dome Summit South ice core, Law Dome, East Antarctica, *Earth System Science Data*, 8, 253–263, doi:10.5194/essd-8-253-2016, 2016.
- 15 Trickett, Y., Baker, I., and Pradhan, P.: The orientation dependence of the strength of ice single crystals, *J. Glaciol.*, 46, 41–44, doi:10.3189/172756500781833296, 2000.
- van der Veen, C. J. and Whillans, I. M.: Force budget: I. Theory and numerical methods, *J. Glaciol.*, 35, 53–60, 1989.
- van der Veen, C. J. and Whillans, I. M.: Development of fabric in ice, *Cold Reg. Sci. Technol.*, pp. 171–195, doi:10.1016/0165-232X(94)90027-2, 1994.
- 20 Wang, W. and Warner, R. C.: Modelling of anisotropic ice flow in Law Dome, East Antarctica, *Ann. Glaciol.*, 29, 184–190, 1999.
- Wang, W., Warner, R. C., and Budd, W. F.: Ice-flow properties at Dome Summit South, Law Dome, East Antarctica, *Ann. Glaciol.*, 35, 567–573, 2002a.
- Wang, W., Jun, L., Zwally, H. J., Morgan, V., and van Ommen, T. D.: The effect of anisotropic flow properties on ice-sheet surface elevation change, *Ann. Glaciol.*, 39, 439–444, 2004.
- 25 Wang, W., Li, J., and Zwally, H. J.: Dynamic inland propagation of thinning due to ice loss at the margins of the Greenland ice sheet, *J. Glaciol.*, 58, 734–740, doi:10.3189/2012JoG11J187, 2012.
- Wang, W. L. and Warner, R. C.: Simulation of the influence of ice rheology on velocity profiles and ice-sheet mass balance, *Ann. Glaciol.*, 27, 194–200, 1998.
- Wang, W. L., Zwally, H. J., Abdalati, W., and Luo, S.: Modeling of ice flow and internal layers along a flowline through Swiss Camp, West
- 30 Greenland, *Ann. Glaciol.*, 34, 303–308, 2002b.
- Wang, W. L., Zwally, H. J., Hulbe, C. L., Siegert, M. J., and Joughin, I. R.: Anisotropic ice flow leading to the onset of Ice Stream D, West Antarctica: numerical modelling based on the observations from Byrd Station borehole, *Ann. Glaciol.*, 37, 397–403, 2003.
- Warner, R. C., Jacka, T. H., Li, J., and Budd, W. F.: Tertiary flow relations for compression and shear components in combined stress tests on ice, in: *Advances in cold-region thermal engineering and sciences: technological, environmental, and climatological impact*, edited by
- 35 Hutter, K., Wang, Y., and Beer, H., pp. 259–270, Springer-Verlag, 1999.
- Weertman, J.: Deformation of floating ice shelves, *J. Glaciol.*, 3, 38–42, 1957.
- Winkelmann, R., Martin, M. A., Haseloff, M., Albrecht, T., Bueler, E., Khroulev, C., and Levermann, A.: The Potsdam Parallel Ice Sheet Model (PISM-PIK) - Part 1: Model description, *The Cryosphere*, 5, 715–726, doi:10.5194/tc-5-715-2011, 2011.

Zwinger, T., Schäfer, M., Martín, C., and Moore, J. C.: Influence of anisotropy on velocity and age distribution at Scharffenbergbotnen blue ice area, *The Cryosphere*, 8, 607–621, doi:10.5194/tc-8-607-2014, 2014.

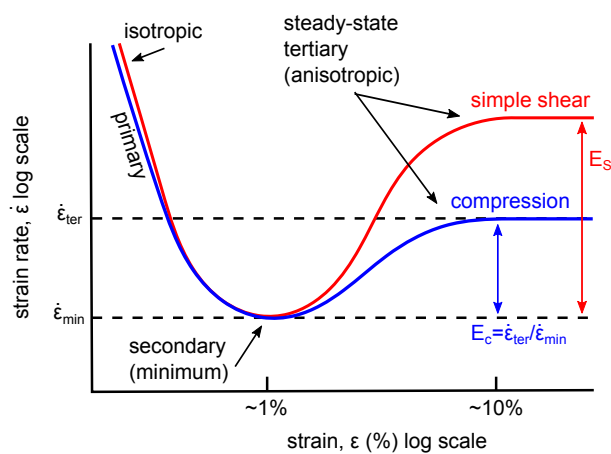


Figure 1. [Strain-Schematic illustrating strain](#) rate characteristics of polycrystalline ice undergoing deformation driven by single stresses as measured in laboratory experiments. The part of the curve corresponding to tertiary (steady-state) anisotropic creep is relevant to the deformation of ice masses in typical ice sheets and glaciers. The red (blue) curve illustrates the result of simple shear-alone (compression-alone) stress configurations. [Note that the](#) [The](#) ratio of the shear enhancement factor E_S to the compression enhancement factor E_C is approximately $8/3$ ([Treverrow et al., 2012](#)), and the enhancement due to compression-alone is approximately three times that of the secondary (minimum) creep rate.

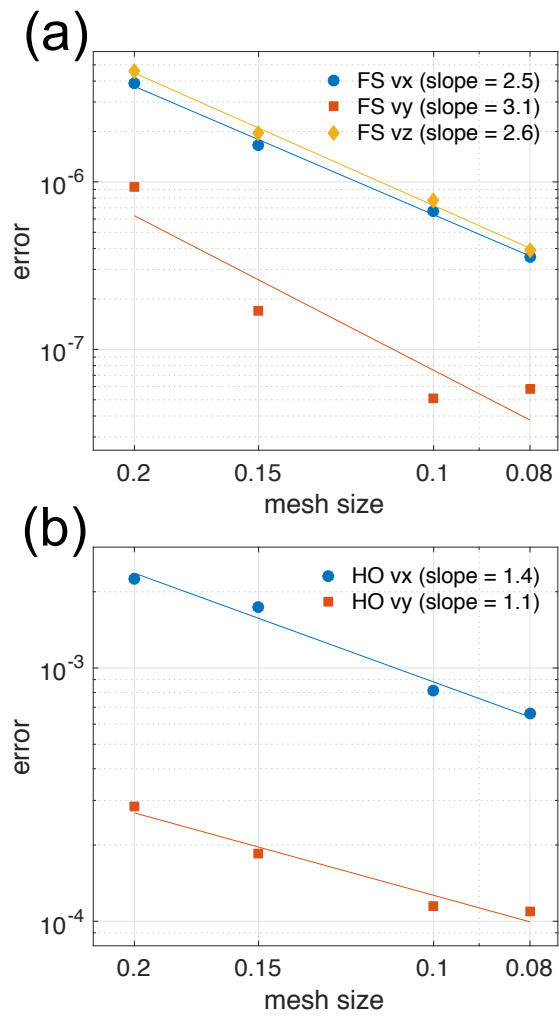


Figure 2. Convergence rates of the simulated (a) full-Stokes (FS) and (b) higher-order (HO) velocity fields (v_x, v_y, v_z) to the analytical solutions in Eqs. 13-17 for increasing mesh resolutions.

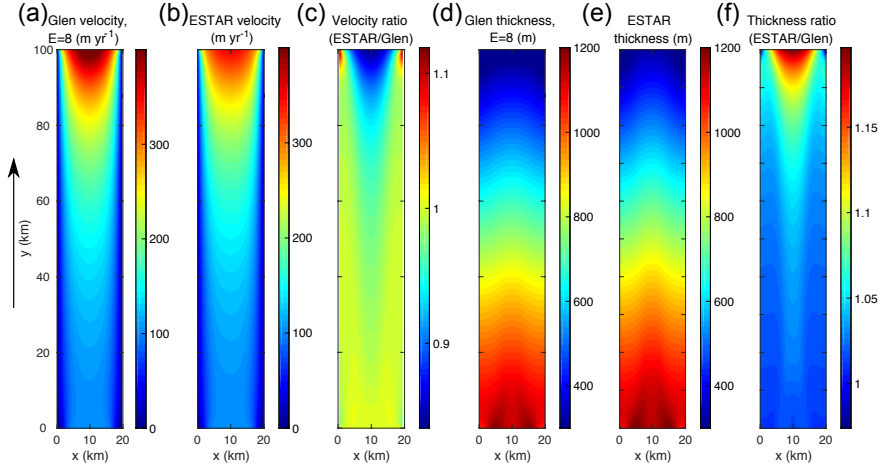


Figure 3. Rectangular ice shelf HO-higher-order steady-state surface fields. (a) Velocity magnitude (m yr^{-1}) for the Glen flow relation ($E_G = 8$); (b) velocity magnitude (m yr^{-1}) for ESTAR; (c) ratios (i.e., ESTAR/Glen) of velocity magnitudes; (d) thickness (m) for the Glen flow relation ($E_G = 8$); (e) thickness (m) for ESTAR; and (f) ratios (i.e., ESTAR/Glen) thicknesses. The black arrow indicates the direction of flow.

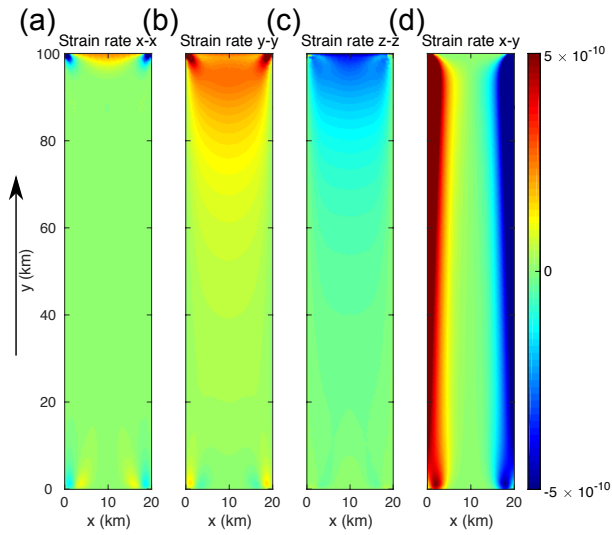


Figure 4. Rectangular ice shelf ESTAR HO-higher-order steady-state surface strain rates (s^{-1}): (a) $\dot{\epsilon}_{xx}$; (b) $\dot{\epsilon}_{yy}$; (c) $\dot{\epsilon}_{zz}$; and (d) $\dot{\epsilon}_{xy}$.

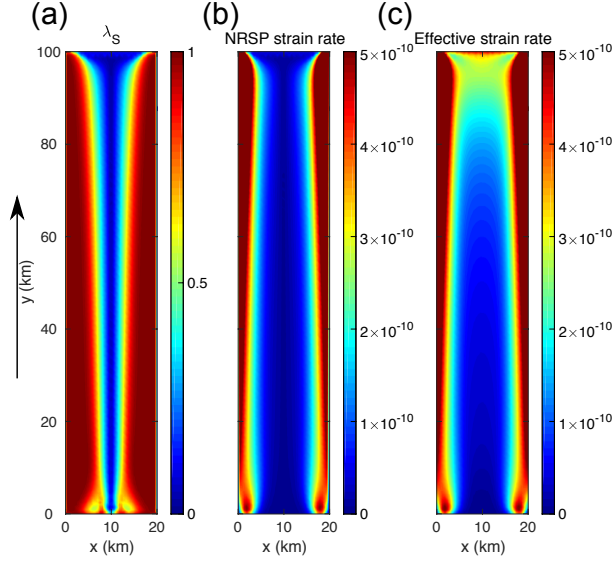


Figure 5. Rectangular ice shelf ESTAR ~~HO-higher-order~~ steady-state surface fields. (a) ESTAR shear ratio λ_S ; (b) shear strain rate resolved on the non-rotating shear plane (NRSP) $\dot{\epsilon}'$ (s^{-1}); and (c) effective strain rate $\dot{\epsilon}_e$ (s^{-1}). The black arrow indicates the direction of flow.

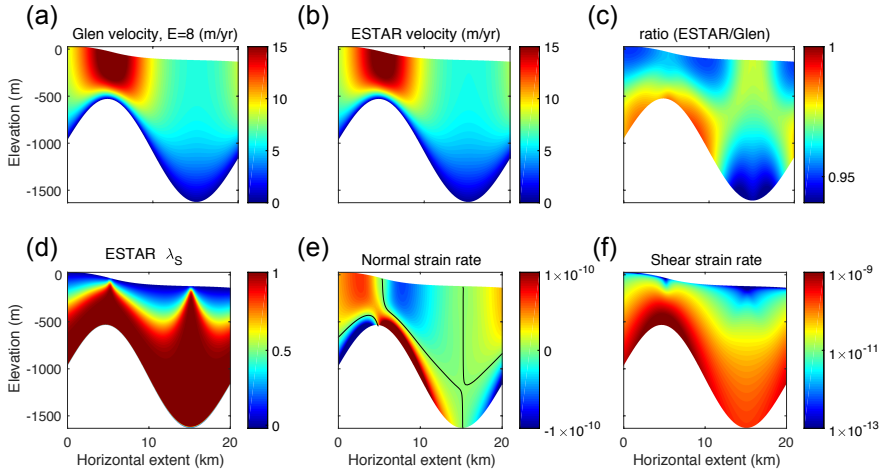


Figure 6. ISMIPB ~~FS-full-Stokes~~ steady-state results with horizontal extent $L = 20$ km. (a) Horizontal velocity v_x ($m\ yr^{-1}$) for the Glen flow relation with $E_G = 8$; (b) v_x ($m\ yr^{-1}$) for ESTAR with $E_S = 8$ and $E_C = 3$; and (c) ratio between the Glen and ESTAR v_x fields; (d) ESTAR shear enhancement factor λ_S (Eq. 6); (e) ESTAR normal strain rate (i.e., $x-x$ strain rate; s^{-1}); and (f) ESTAR shear strain rate (i.e., $x-z$ strain rate; s^{-1}). The black contours in (e) correspond to the curves where $\dot{\epsilon}_{xx} = 0$. Note the log scale in (f).

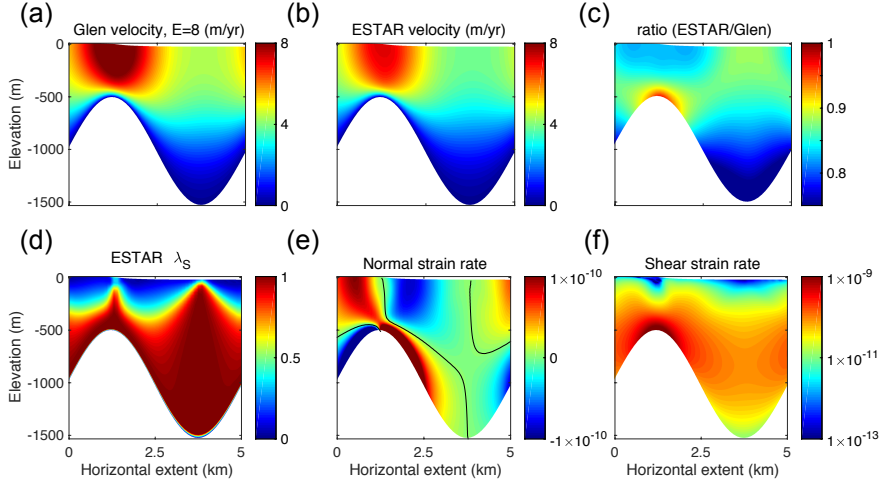


Figure 7. ISMIPB FS-full-Stokes steady-state results with horizontal extent $L = 5$ km. **(a)** Horizontal velocity v_x (m yr^{-1}) for the Glen flow relation with $E_G = 8$; **(b)** v_x (m yr^{-1}) for ESTAR with $E_S = 8$ and $E_C = 3$; and **(c)** ratio between the Glen and ESTAR v_x fields; **(d)** ESTAR shear enhancement factor λ_S (Eq. 6); **(e)** ESTAR normal strain rate (i.e., $x-x$ strain rate; s^{-1}); and **(f)** ESTAR shear strain rate (i.e., $x-z$ strain rate; s^{-1}). The black contours in **(e)** correspond to the curves where $\dot{\epsilon}_{xx} = 0$. Note the log scale in **(f)**.

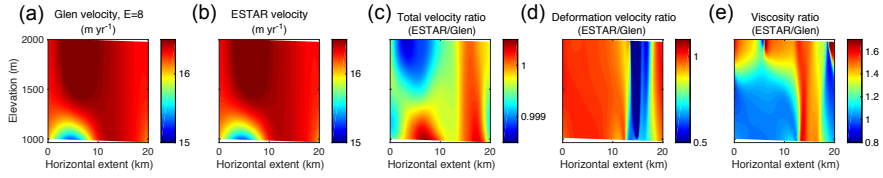


Figure 8. ISMIPD FS-full-Stokes steady-state results with horizontal extent $L = 20$ km. **(a)** Glen horizontal velocities v_x (m yr^{-1}); **(b)** ESTAR v_x (m yr^{-1}); **(c)** ratios of ESTAR/Glen v_x ; **(d)** ratios of ESTAR/Glen deformation velocities (i.e., the difference between v_x and the sliding velocity, which is taken to be equal to the velocity along the basal mesh points); and **(e)** ratios of ESTAR/Glen viscosities.

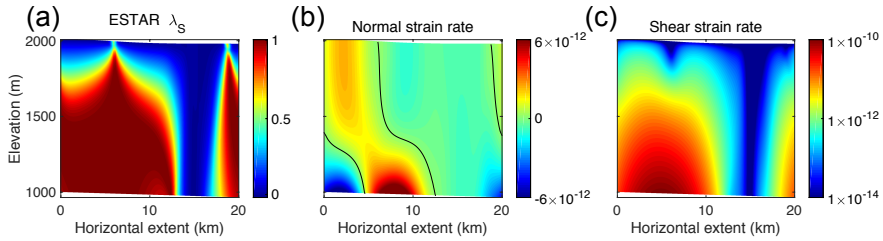


Figure 9. ISMIPD ESTAR FS-full-Stokes steady-state enhancement factors and normal and shear strain rates with horizontal extent $L = 20$ km. **(a)** λ_S ; **(b)** normal strain rates (s^{-1}); and **(c)** shear strain rates (s^{-1}). The black contour lines in **(b)** correspond to the curves where $\dot{\epsilon}_{xx} = 0$. Note the log scale in **(c)**.

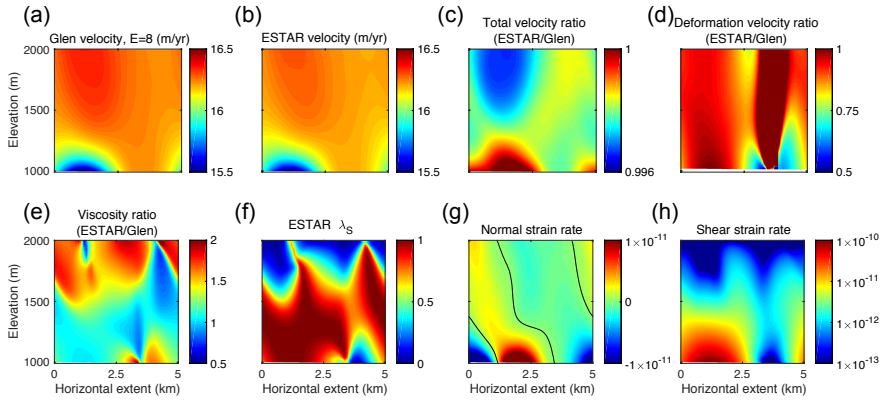


Figure 10. ISMIPD ~~FS~~-full-Stokes steady-state results with horizontal extent $L = 5$ km. (a) Glen horizontal velocity v_x (m yr^{-1} , with $E_G = 8$); (b) ESTAR v_x (m yr^{-1}); (c) ratio of ESTAR/Glen v_x ; (d) ratio of ESTAR/Glen deformation v_x ; (e) ratio of ESTAR/Glen viscosity; (f) ESTAR λ_S ; (g) ESTAR normal strain rate (s^{-1}); and (h) ESTAR shear strain rate (s^{-1}). The black contours in (g) correspond to the curves where $\dot{\epsilon}_{xx} = 0$. Note the log scale in (h).

Table 1. Computational times for full-Stokes simulations of the embayed ice shelf (Sect. 6.1) using Glen and ESTAR [flow relations](#) for increasing mesh resolution. The model is simulated for 1 month and for a total of 833 time steps in each case. Dof stands for model degrees of freedom.

Dof	Vertices	CPUs	Glen walltime (s)	ESTAR walltime (s)
2210	10040	16	9084	9281
2760	15665	32	10467	10778
3310	22540	64	12920	13008
4410	40040	128	20852	21008
8820	80080	256	59057	59934